PHYS2082 Content Notes

Ryan White
s4499039

Semester 2, 2021

This document consists of a summarised recording of text taken from *"An Introduction to Modern Astrophysics – Second Edition"* [Carrol, B & Ostlie, D], taken in the context of content relevant to PHYS2082 at UQ. These notes were typed under core-crushing pressure of course failure [heh], and consequently *may* have been rushed. If you believe this is the case, no you don't.

Worth noting is that these notes don't take into account the information given specifically in the course's accompanying lectures and serve only as a "summary" of the textbook in the context of the course's aims. I'm sure you'll notice that some topics have been regrettably glossed over, while some others have comparatively too much detail. In any case, I hope you'll find this useful and should you see any errors, I'm sure that you can find me somehow.

Contents

1 Week 1 - Orbits, Parallax and Magnitude

2.1 - Elliptical Orbits

Kepler pioneered elliptical orbits as opposed to circular orbits

Kepler's First Law: A planet orbits the sun in an ellipse, with the sun at one focus of the ellipse.

Kepler's Second Law: A line connecting a planet to the sun sweeps out equal areas in equal time intervals.

Kepler's Third Law: The periodicity of a planet in orbit of the sun is related to its semi-major axis by

$$P^2 = a^3$$

where P is the orbital period (years), and a is the semi-major axis. (This is strictly for the *solar system.*)

An astronomical unit is defined as 1.496×10^{11}m.

The Geometry of Elliptical Motion

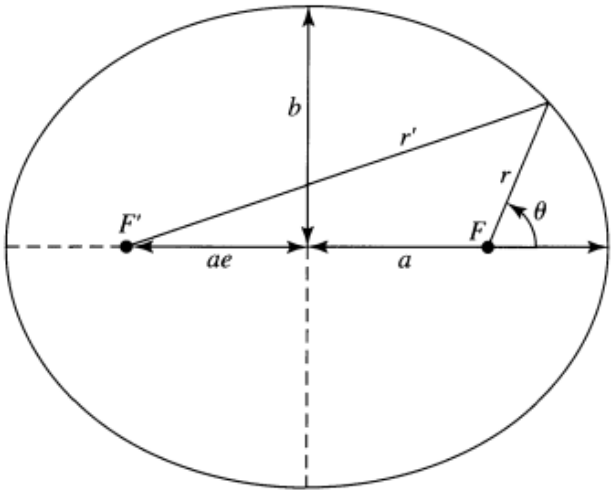

Figure 2.4: Geometry of an Ellipse

An ellipse is defined by that set of points that satisfy
$r + r' = 2a.$ (2.1)
The sun is located at the principle focus, F.
The distance b is the semi-major axis and a the semi-major axis. The eccentricity, e $(0 \leq e \leq 1)$ of the ellipse is defined as the distance between the foci divided by the semi-major axis.
The axes values are related to each other by
$b^2 = a^2(1 - e^2)$ (2.2)
The area of an ellipse is $A = \pi ab$ (2.4)
The distance from the principle focus at any point along the ellipse is calculated by

$$r = \frac{a(1 - e^2)}{1 + e\cos\theta} \tag{2.3}$$

$e = 0$ corresponds to a circle, $e = 1$ a parabola and $e > 1$ a hyperbola.

2.2 - Newtonian Mechanics

Kepler's First Law

The path of the reduced mass ($\mu = (m_1 m_2)/(m_1 + m_2)$) about the center of mass under the influence of gravity is a conic section.

$$r = \frac{L^2/\mu^2}{GM(1 + e\cos\theta)} \tag{2.29}$$

Elliptical orbits result from gravity when the total energy of the system is less than zero.
Kepler's first law for bounded planetary orbits states: *"Both objects in a binary orbit move about the center of mass in ellipses, with the center of mass occupying one focus of each ellipse."*
The total angular momentum of the system is $L = \mu\sqrt{GMa(1 - e^2)}$ (2.30)

Kepler's Second Law

The time rate of change of the area swept out by a line connecting a planet to the focus of an ellipse is a constant:

$$\frac{dA}{dt} = \frac{1}{2}\frac{L}{\mu} \tag{2.32}$$

The orbital speeds at perihelion, aphelion, and at any radius in the orbit are

$$v_p^2 = \frac{GM(1+e)}{r_p} = \frac{GM}{a}\left(\frac{1+e}{1-e}\right) \tag{2.33}$$

$$v_a^2 = \frac{GM(1-e)}{r_a} = \frac{GM}{a}\left(\frac{1-e}{1+e}\right) \tag{2.34}$$

$$v^2 = G(m_1+m_2)\left(\frac{2}{r} - \frac{1}{a}\right) \tag{2.36}$$

Kepler's Third Law

The general form of Kepler's third law, for any binary system, is

$$\boxed{P^2 = \frac{4\pi^2}{G(m_1+m_2)}a^3} \tag{2.37}$$

where P is in seconds, and a in meters.

2.4 - The Virial Theorem

For gravitationally bound systems in equilibrium, the total energy is always one half of the time averaged potential energy. Or rather, the kinetic energy of the system is half the negated value of the potential energy. That is,

$$\langle E\rangle = \frac{1}{2}\langle U\rangle \qquad \Rightarrow \qquad -2\langle K\rangle = \langle U\rangle \tag{2.46 \& 2.47}$$

3.1 - Stellar Parallax

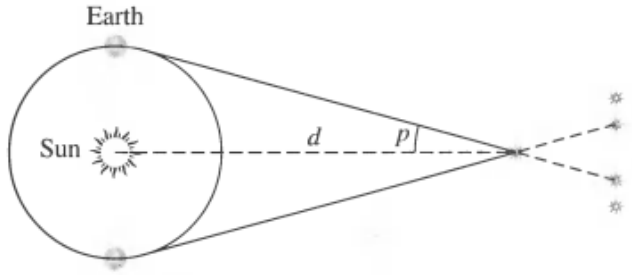

Figure 3.2: Stellar Parallax

Trigonometric parallax involves measuring an object's angular position from two observation points separated by a known baseline distance. A measurement of parallax angle, p (one half of the maximum change in angular position) allows the calculation of the distance to the star

$$d = \frac{1\text{ AU}}{\tan p} \approx \frac{1}{p}\text{ AU}$$

Define a new unit of distance, the parallax second, or parsec as 1 pc $= 2.0626 \times 10^5$ AU $= 3.0857 \times 10^{16}$m

This leads to

$$\boxed{d = \frac{1}{p"}\text{ pc}} \tag{3.1}$$

where p" is in units of arcseconds.

3.2 - The Magnitude Scale

Apparent Magnitude

Apparent magnitude measures how bright stars appear to be from the observer's perspective. A difference in 1 magnitude corresponds to a brightness ratio of $100^{1/5} \approx 2.512$. Thus, a first magnitude star is $2.512^2 = 6.31$ times brighter than a third magnitude star, etc. The magnitude scale ranges currently from -26.83 (for the Sun) to about $m = 30$ for the faintest object detectable.

Flux, Luminosity and the Inverse Square Law

The brightness of a star is actually measured in terms of the radiant flux, F. Radiant flux is the wattage of starlight received by 1 square meter of a detector aimed at the star, and depends on the intrinsic luminosity (energy emitted per second) and the distance from the observer.
Radiant flux measured at a distance r is related to the stars luminosity, L, by

$$\boxed{F = \frac{L}{4\pi r^2}} \tag{3.2}$$

It's clear that the radiant flux is inversely proportional to the square of the distance from the star. This is the inverse square law for light.

Absolute Magnitude

The absolute magnitude of a star is what it's apparent magnitude would be if it were located at a distance of 10pc from the observer, and is denoted M.
The flux ratio of two stars of apparent magnitudes m_1 and m_2 are

$$\frac{F_2}{F_1} = 100^{(m_1 - m_2)/5} \tag{3.3}$$

The Distance Modulus

The connection between distance and apparent and absolute magnitude of a star is

$$\boxed{d = 10^{(m-M+5)/5} \text{ pc}} \tag{3.5}$$

The quantity $m - M$ is a measure of distance to a star and is called the distance modulus:

$$\boxed{m - M = 5\log_{10} d - 5 = 5\log_{10}\left(\frac{d}{10\text{pc}}\right)} \tag{3.6}$$

The luminosity ratio of two stars is then

$$\frac{L_2}{L_1} = 100^{(M_1 - M_2)/5} \tag{3.7}$$

Letting one of the stars be the Sun reveals the relationship between a star's absolute magnitude and its luminosity:

$$\boxed{M = M_\odot - 2.5\log_{10}\left(\frac{L}{L_\odot}\right)} \tag{3.8}$$

2 Week 2 - Blackbody, Albedo and Redshift

3.4 - Blackbody Radiation

The Connection between Colour and Temperature

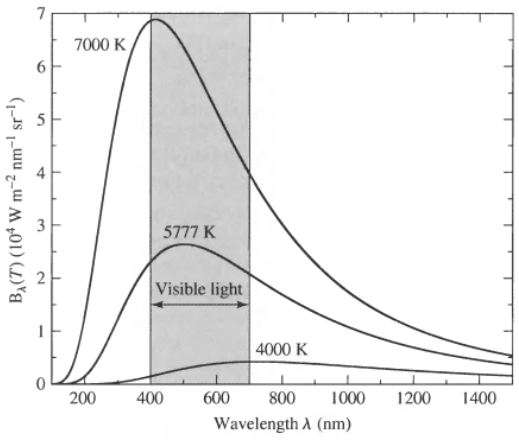

Figure 3.8: Blackbody Spectrum

An ideal emitter is an object that absorbs all of the incident light energy and re-radiates this energy with the characteristic spectrum. Because the ideal emitter reflects no light, it is known as a blackbody, and the radiation it emits is blackbody radiation. Stars are approximated (to varying degrees of accuracy) as blackbodies.
A blackbody of temperature T emits a continuous spectrum, with a peak at $\lambda_{\max}$.
Wien's displacement law relates T with $\lambda_{\max}$ by

$$\lambda_{\max} T = 0.002897755\text{mK} \tag{3.15}$$

The Stefan-Boltzmann Equation

Figure 3.8 shows that as the temperature increases, it emits more energy per second at *all* wavelengths. For a spherical star of radius R and surface area $A = 4\pi R^2$, the Stefan-Boltzmann Equation is

$$\boxed{L = 4\pi R^2 \sigma {T_e}^4} \tag{3.17}$$

This relates luminosity to the effective temperature of a stars surface. Combining this with the inverse square law shows that the surface flux of a star is

$$F_{\text{surf}} = \sigma T_e^4 \tag{3.18}$$

3.6 - The Colour Index

The apparent and absolute magnitudes of a star, measured over all wavelengths of light emitted by a star, are known as **bolometric magnitudes**, and are denoted m_{bol} and M_{bol} respectively.

UBV Wavelength Filters

In the standard UBV system, a star's apparent magnitude is measured through three filters and is designated by three capital letters:

- U: the star's ultraviolet magnitude (centered at 365nm with an effective band width of 68nm)
- B: the star's blue magnitude (centered at 440nm, bandwidth of 98mm)
- V: the star's visual magnitude (550nm, bandwidth of 89mm)

Colour Indices and the Bolometric Correction

A star's $U-B$ colour index is the difference between it's ultraviolet and blue magnitudes, and a star's $B-V$ colour index is the difference between it's blue and visual magnitudes:

$$U - B = M_V - M_B$$
$$B - V = M_B - M_V$$

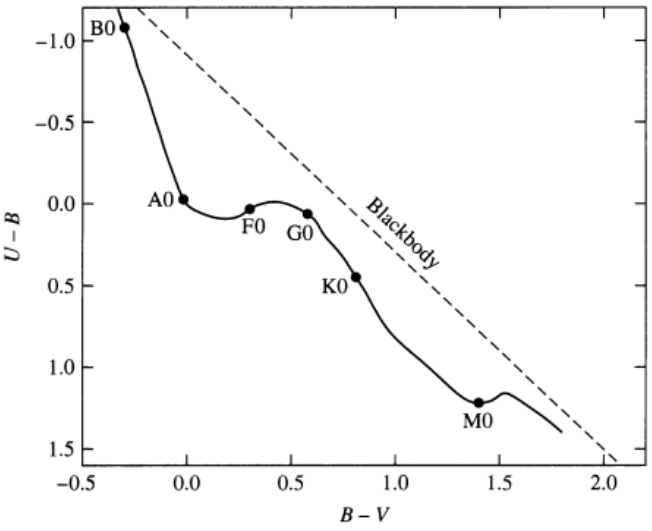

Figure 3.11: Colour-Colour Diagram for Main-Sequence Stars

A smaller $B-V$ index means that a star is bluer. The difference between a star's bolometric and visual magnitudes is it's bolometric correction, BC:

$$\boxed{BC = m_{\text{bol}} - V = M_{\text{bol}} - M_V} \tag{3.30}$$

The Colour-Colour Diagram

Since stars aren't perfect black bodies, they don't follow a linear relationship on a colour-colour diagram.

Figure 3.11 shows that the blackbody approximation is best for very cool, very hot, and intermediate temperature stars.

19.3 - The Physics of Atmospheres

The Temperatures of the Planets

Under equilibrium conditions, a planet's total energy content remains constant. Therefore, all absorbed energy must be re-emitted. For simplicity, assume a planet's temperature is uniform across its surface, and the planet reflects a portion (the albedo) of incident light. Using this approximation, the temperature of the planet can be shown to be

$$\boxed{T_P = T_{\text{star}}(1-a)^{1/4}\sqrt{\frac{R_{\text{star}}}{2D}}} \tag{19.5}$$

where T_{star} and R_{star} are the temperature of the parent star, D is the planet's distance from the star, and a is the planet's albedo.

4.3 - Time and Space in Special Relativity

Relativistic Doppler Shift

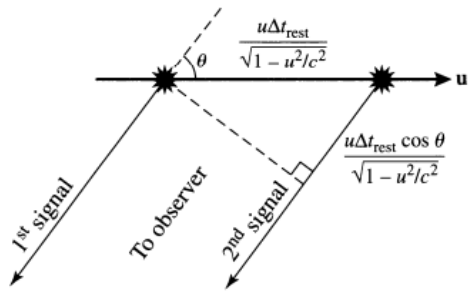

Figure 4.9: Relativistic Doppler Shift

As a wave moves through a medium, the wavelength is compressed in the forward direction and expanded in the backward direction. Classical doppler shift is inaccurate for light. Relativistic doppler shift is described by

$$\boxed{\nu_{\text{obs}} = \frac{\nu_{\text{rest}}\sqrt{1-u^2/c^2}}{1+(u/c)\cos\theta} = \frac{\nu_{\text{rest}}\sqrt{1-u^2/c^2}}{1+v_r/c}} \tag{4.32}$$

where $v_r = u\cos\theta$ is the radial velocity of the light source, and u is the relative velocity. If the light source is moving away from the observer, then $\lambda_{\text{obs}} < \lambda_{\text{rest}}$, where the rest subscript refers to the source reference frame.

Conversely, if the source is moving toward the observer, then $\lambda_{\text{obs}} < \lambda_{\text{rest}}$. This is **redshift** and **blueshift** respectively. A redshift parameter, z, is used to describe the change in wavelength by

$$z \equiv \frac{\lambda_{\text{obs}} - \lambda_{\text{rest}}}{\lambda_{\text{rest}}} = \frac{\Delta\lambda}{\lambda_{\text{rest}}} \tag{4.34}$$

If the source is moving directly towards or away from the observer (radial motion), then

$$v_{\text{obs}} = v_{\text{rest}}\sqrt{\frac{1 - v_r/c}{1 + v_r/c}} \qquad z = \sqrt{\frac{1 + v_r/c}{1 - v_r/c}} - 1 \tag{4.35 \& 4.36}$$

In general,

$$z = \frac{\Delta t_{\text{obs}}}{\Delta t_{\text{rest}}} - 1 \tag{4.37}$$

5.1 - Spectral Lines

Kirchhoff's Laws

- A hot, dense gas or hot solid object produces a continuous spectrum with no dark spectral lines
- A hot, diffuse gas produces bright spectral lines (emission lines)
- A cool, diffuse gas in front of a source of a continuous spectrum produces dark spectral lines (absorption lines) in the continuous spectrum

Applications of Stellar Spectra Data

For individual stars, $v_r \ll c$, and so a low-speed approximation of relative radial velocity is

$$\boxed{\frac{\lambda_{\text{obs}} - \lambda_{\text{rest}}}{\lambda_{\text{rest}}} = \frac{\Delta\lambda}{\lambda_{\text{rest}}} \simeq \frac{v_r}{c}} \tag{5.1}$$

5.3 - The Bohr Model of the Atom

Bohr's Semi-Classical Atom

The allowed energies of the Bohr atom are (for n principle quantum number):

$$E_n = -\frac{\mu e^4}{32\pi^2\epsilon_0^2\hbar^2}\frac{1}{n^2} = \frac{1}{n^2}\cdot -13.6\text{eV} \tag{5.14}$$

For an atom going from a high energy state to a low one,

$$E_{\text{photon}} = E_{\text{high}} - E_{\text{low}} = \frac{hc}{\lambda}$$

which gives, for Hydrogen,

$$\frac{1}{\lambda} = R_H\left(\frac{1}{{n_{\text{low}}}^2} - \frac{1}{{n_{\text{high}}}^2}\right) \tag{5.15}$$

where $R_H \simeq 1.097 \times 10^7\ \text{m}^{-1}$

3 Week 3 - Binary Systems

7.1 - The Classification of Binary Stars

The only direct way to measure the mass of a star is by studying its gravitational influence on other objects. Binary star systems are classified according to their specific observational characteristics:

Optical Double: These systems are not actually binaries, but simply two stars along the same line of sight (i.e. they have similar right ascensions and declinations). These stars are not gravitationally bound and so mass cannot be determined.

Visual Binary: Both stars in the binary can be resolved independently. If the orbital period isn't prohibitively long, the motion of each star can be determined. These systems provide data about the angular separation of stars from their mutual center of mass. If the distance to the binary is known, linear separation can be found.

Astrometric Binary: If one of the objects is significantly brighter than the other, it may not be possible to resolve the dimmer object. In this case, the properties of the dim object can be deduced by observing the oscillatory motion of the bright object.

Eclipsing Binary: For binaries that have orbital planes oriented along the line of sight of the observer, one star will periodically pass in front of the other, blocking the light of the eclipsed component. Such a system is recognizable by regular light fluctuations in a telescope. The data can provide information about the relative effective temperatures and radii of each star.

Spectrum Binary: A spectrum binary is a system with two superimposed, independent, discernible spectra. The Doppler effect causes the spectral lines of a star to be shifted if it has non-zero radial velocity. Since the stars are continuously in motion about the center of mass, there will be periodic shifts in the wavelengths of each spectral line.
If one star's spectra is blueshifted, the other must be redshifted.
However, the orbital period may be so long that the time dependence of spectral wavelengths isn't apparent. Even if Doppler shifts aren't significant, it may be possible to detect two sets of superimposed spectra if they originate from stars that have significantly different spectral features.

Spectroscopic Binary: If the orbital period of a binary isn't prohibitively long and the motion has a component along the line of sight, a period shift in spectral lines will be observable. If both of the luminosities are comparable, both spectra will be observable. If one star is much more luminous, then the spectrum of the less luminous companion will be overwhelmed and only a single set of periodically varying spectral lines will be seen.

These specific classifications are not mutually exclusive. Three types of systems can help with mass determinations:

- Visual binaries combined with parallax observations
- Visual binaries where radial velocities are available over a complete orbit
- Eclipsing, double line, spectroscopic binaries

7.2 - Mass Determination using Visual Binaries

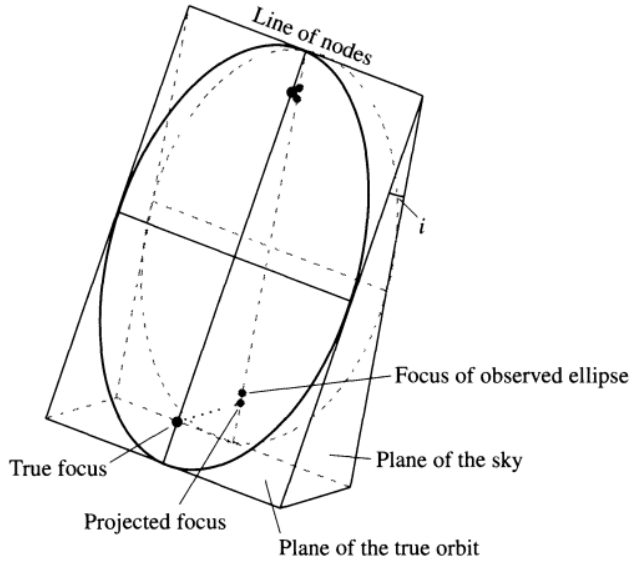

Figure 7.4: Geometry of Inclined Orbits

The ratio of masses of two stars in a binary is equal to that of the inverse ratio of their angular distance from the mutual center of mass (measured in radians). That is,

$$\boxed{\frac{m_1}{m_2} = \frac{\alpha_2}{\alpha_1}} \tag{7.2}$$

Let i be the **angle of inclination** between the plane of an orbit and the plane of the sky. As a special case, assume that the orbital plane and the plane of the sky (defined as being perpendicular to the line of sight) intersect along a line parallel to the minor axis, forming a **line of nodes**. The observer measures the angle as $\tilde{\alpha}_1 = \alpha_1 \cos i$ and $\tilde{\alpha}_2 = \alpha_2 \cos i$, where $\tilde{\alpha}_1$ denotes the observed angular separation and α_1 the actual angular separation.
The masses of the two stars are then

$$\boxed{m_1 + m_2 = \frac{4\pi^2}{G}\frac{(\alpha d)^3}{P^2} = \frac{4\pi^2}{G}\left(\frac{d}{\cos i}\right)^3 \frac{\tilde{\alpha}^3}{P^2}} \tag{7.3}$$

where $\tilde{\alpha} = \tilde{\alpha}_1 + \tilde{\alpha}_2$

7.3 - Eclipsing, Spectroscopic Binaries

The Effect of Eccentricity on Radial Velocity Measurements

For a star system having circular orbits, the speed of each star will be constant. If the plane of their orbits lies in the line of sight of the observer ($i = 90^o$), the measured radial velocities will produce sinusoidal velocity curves. Changing the inclination doesn't change the shape of the curve, only the amplitudes by a factor of $\sin i$.
When the eccentricity, e, of the orbits are not zero, the observed velocity curves become skewed.

The Mass Function and the Mass-Luminosity Relation

Assuming that the eccentricity is very small ($e \ll 1$), then the speeds of the stars are essentially constant and are described by

$$v_1 = \frac{2\pi a_1}{P} \qquad v_2 = \frac{2\pi a_2}{P}$$

The observed radial velocities, $v_{1r} = v_1 \sin i$; $v_{2r} = v_2 \sin i$, can be used to show the mass ratio:

$$\boxed{\frac{m_1}{m_2} = \frac{v_2}{v_1} = \frac{v_{2r}/\sin i}{v_{1r}/\sin i} = \frac{v_{2r}}{v_{1r}}} \qquad (7.4 \text{ \& } 7.5)$$

The sum of the masses can also be found using observed values by

$$\boxed{m_1 + m_2 = \frac{P}{2\pi G}\frac{(v_{1r} + v_{2r})^2}{\sin^3 i}} \qquad (7.6)$$

If one star is much brighter than the other, the system is referred to as a single-line spectroscopic binary. This means that the radial velocity of only the brighter star may be measured and so

$$\boxed{\frac{m_2^3}{(m_1 + m_2)}^2 \sin^3 i = \frac{P}{2\pi G} v_{1r}^3} \qquad (7.7)$$

This is known as the **mass function**, and the RHS relies only on observable quantities. It is only useful if the mass of one of the bodies is already known.
Evaluating masses of binaries has shown the existence of a well-defined, linear **mass-luminosity relation** for the large majority of main-sequence stars in the sky.

Using Eclipses to Determine Radii and Ratios of Temperatures

An eclipsing system implies i is close to 90^o. If if it is not 90^o, the error as a result is small.
If the smaller star is completely eclipsed by the larger one, a nearly constant minimum will occur in the measured brightness of the system during oscillation. Assuming $i \simeq 90^o$, the radius of the smaller star can be calculated. Let t_a be the time of first contact, t_b the time of minimum light, and r_s be the small star radius. Then,

$$r_s = \frac{v}{2}(t_b - t_a) \qquad (7.8)$$

where $v = v_s + v_l$ is the relative velocity of the two stars. If t_c is the time at which the total flux begins rising, then the radius of the large star is

$$r_l = \frac{v}{2}(t_c - t_a) = r_s + \frac{v}{2}(t_c - t_b) \qquad (7.9)$$

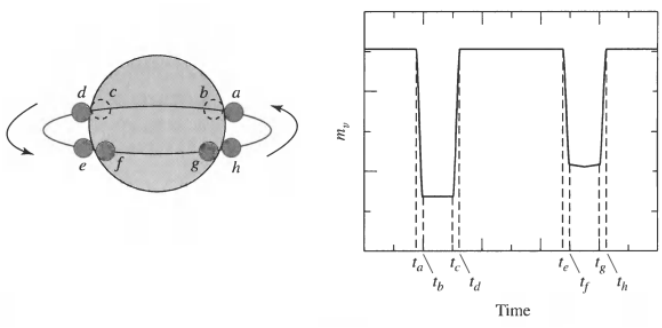

Figure 7.9: Light Curve of an Eclipsing Binary

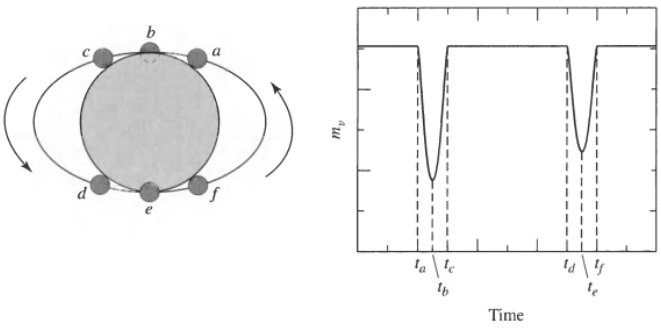

Figure 7.10: Light Curve of a Partially Eclipsing Binary

The ratio of effective temperatures of the two stars can also be obtained from the light curve of an eclipsing binary. The dip in the light curve is deeper when a smaller, hotter star is passing behind its companion. Recall that the radiative surface flux is given by $F_{\text{surf}} = \sigma T_e^4$.

Let B_0 be the light detected from the binary when both stars are visible. The deeper, or primary, minimum (B_p) occurs when the hotter star passes behind the cooler one. If the smaller star is hotter, the light received during the primary minimum is just due to the larger, cooler star. The light received at the secondary minimum (B_s) is then the light from the smaller, hotter star as well as the light from the larger star minus the cross section of the smaller star. It follows that

$$\boxed{\frac{B_0 - B_p}{B_0 - B_s} = \frac{F_{rs}}{F_{rl}} = \left(\frac{T_s}{T_l}\right)^4} \qquad (7.10 \ \& \ 7.11)$$

7.4 - The Search for Extrasolar Planets

Given the disparity between the luminosity of a star and its orbiting planets, direct observation of an exoplanet is rare. Three techniques are mainly used to observe exoplanets: radial velocity measurements, astrometric wobbles, and eclipses.

4 Week 4 - Stellar Classification and Ionization

8.1 - The Formation of Spectral Lines

The Spectral Types of Stars

Spectral Type	Characteristics
O	Hottest blue-white stars with few lines Strong He II absorption (sometimes emission) lines. He I absorption lines becoming stronger.
B	Hot blue-white He I absorption lines strongest at B2. H I (Balmer) absorption lines becoming stronger.
A	White Balmer absorption lines strongest at A0, becoming weaker later. Ca II absorption lines becoming stronger.
F	Yellow-white Ca II lines continue to strengthen as Balmer lines continue to weaken. Neutral metal absorption lines (Fe I, Cr I).
G	Yellow Solar-type spectra. Ca II lines continue becoming stronger. Fe I, other neutral metal lines becoming stronger.
K	Cool orange Ca II H and K lines strongest at K0, becoming weaker later. Spectra dominated by metal absorption lines.
M	Cool red Spectra dominated by molecular absorption bands, especially titanium oxide (TiO) and vanadium oxide (VO). Neutral metal absorption lines remain strong.
L	Very cool, dark red Stronger in infrared than visible. Strong molecular absorption bands of metal hydrides (CrH, FeH), water (H_2O), carbon monoxide (CO), and alkali metals (Na, K, Rb, Cs). TiO and VO are weakening.
T	Coolest, Infrared Strong methane (CH_4) bands but weakening CO bands.

Table 8.1: Harvard Spectral Classification

The Harvard Classification scheme of "O B A F G K M" is a temperature sequence running from the hottest O stars to the coolest M stars. Stars near the beginning of the sequence are referred to as *early-type* stars and those close to the end as *late-type* stars. These labels also distinguish stars within the spectral subdivisions, so astronomers may refer to a K0 star as "an early K star", and so on.
The distinctions between the spectra of stars with different temperatures are due to the electrons occupying different orbitals in the atmospheres of these stars. Table 8.1 lists some of the defining criteria for various spectral types. Note that the term *metal* is used to indicate any element heavier than helium.

Table 8.1 also includes recently defined spectral types of the very cool stars of spectral classification *T Tauri* and *brown dwarf*.

The Maxwell-Boltzmann Velocity Distribution

Statistical mechanics describes in what orbitals electrons are most likely to be found, and the relative numbers of atoms that are in various stages of ionization.
For a gas in thermal equilibrium, the Maxwell-Boltzmann velocity distribution function describes the fraction of particles having a given range of speeds.

The number of gas particles per unit volume having such speeds between v and $v + dv$ is

$$\boxed{n_v dv = n\left(\frac{m}{2\pi kT}\right)^{3/2} e^{-\frac{mv^2}{2kT}} 4\pi v^2 dv} \tag{8.1}$$

where n is the total number density (particles per unit volume), $n_v \equiv \partial n/\partial V$, m is the particle mass, and T is the temperature of the gas.
It is difficult for a significant number of particles to have an energy much greater or less than the thermal energy; the distribution peaks when these energies are equal at a **most probable speed**:

$$v_{mp} = \sqrt{\frac{2kT}{m}} \tag{8.2}$$

The high-speed exponential tail of the distribution function results in a somewhat higher (average) **root-mean-square speed** of

$$\boxed{v_{\text{rms}} = \sqrt{\frac{3kT}{m}}} \tag{8.3}$$

The Boltzmann Equation

Orbitals of higher energy are less likely to be occupied by electrons. Let s_a stand for the set of quantum numbers $\{n, l, m_l, m_s\}$ that identifies a state of energy E_a for a system of particles. Similarly, let s_b correspond to another

state E_b. The ratio of the probability that the system is in the state s_b compared to the state s_a is given by

$$\frac{P(s_b)}{P(s_a)} = \frac{e^{-E_b/kT}}{e^{-E_a/kT}} = e^{-(E_b-E_a)/kT} \tag{8.5}$$

It's often the case that the energy levels of the system may be **degenerate**, with more than one quantum state having the same energy. That is, if states s_a and s_b are degenerate, then $E_a = E_b$ but $s_a \neq s_b$.
Define g_a to be the number of states with energy E_a. Similarly, define g_b in the same way. These are called the **statistical weights** of the energy levels.
Stellar atmospheres contain a vast number of atoms, so the ratio of probabilities (that a system is in a specific state) is indistinguishable from the ratio of the number of atoms. So, the ratio of the number of atoms N_b with energy E_b to the number of atoms N_a with energy E_a in different states of excitation is given by the Boltzmann equation:

$$\boxed{\frac{N_b}{N_a} = \frac{g_b\ e^{-E_b/kT}}{g_a\ e^{-E_a/kT}} = \frac{g_b}{g_a} e^{-(E_b-E_a)/kT}} \tag{8.6}$$

The Saha Equation

What is responsible for the diminishing strength of the Balmer lines at higher temperatures? The answer lies in considering the relative number of atoms in different states of ionization.

The **partition function**, Z, is the weighted sum of the number of ways the atom can arrange its electrons with the same energy, with more energetic (and thus less likely) configurations receiving less weight from the Boltzmann factor when the sum is taken.
If E_j is the energy of the jth level, and g_j is the degeneracy of that level, then,

$$Z = \sum_{j=1}^{\infty} g_j\ e^{-(E_j-E_1)/kT} \tag{8.7}$$

If we use the partition functions Z_i and Z_{i+1} for the atom in its initial and final stages of ionization, the ratio of the number of atoms in stage $i+1$ to the number of atoms in stage i is the **Saha equation**:

$$\boxed{\frac{N_{i+1}}{N_i} = \frac{2Z_{i+1}}{n_e Z_i} \left(\frac{2\pi m_e kT}{h^2}\right)^{3/2} e^{-\chi_1/kT} = \frac{2kTZ_{i+1}}{P_e Z_i} \left(\frac{2\pi m_e kT}{h^2}\right)^{3/2} e^{-\chi_1/kT}} \tag{8.8 \& 8.9}$$

where χ_1 is the energy needed to ionize the atom (13.6eV for HI atom), and n_e is the number density of free electrons (number of free electrons per unit volume).
Note that as n_e increases, the number of atoms in a higher state of ionization increases.

The narrow region inside a star where hydrogen is partially ionized is called a hydrogen **partial ionization zone** and has a characteristic temperature of approximately 10000K for a wide range of stellar parameters.

5 Week 5 - HR and Stellar Opacity

8.2 - Hertzprung-Russel Diagram

An Enormous Range in Stellar Radii

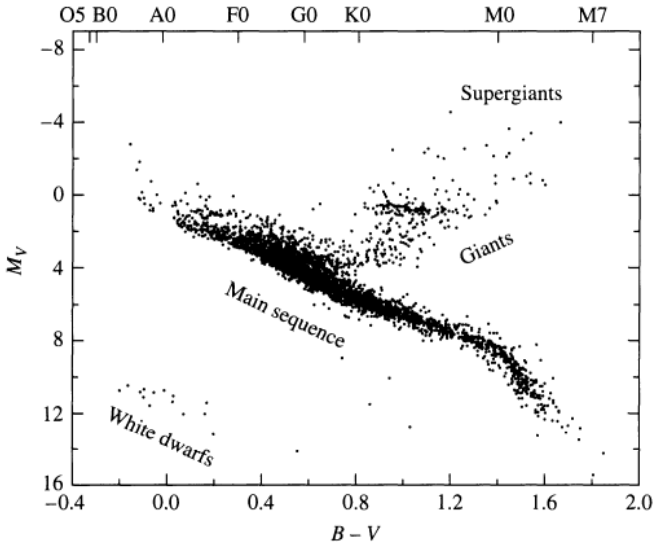

Figure 8.13: An Observer's HR Diagram

If two stars have the same temperature, then the more luminous one must be larger.
The main sequence contains about 80–90% of all stars in the Hertzprung–Russell Diagram, a plot of stellar luminosity (or magnitude) against its colour (or temperature).
Giant stars occupy the region above the main sequence, with supergiants primarily occupying the upper right-hand corner of the HR diagram.
Dwarf stars typically lie beneath the main sequence.
The radius of a star can be easily determined from its position on the HR diagram:

$$R = \frac{1}{T_e^2}\sqrt{\frac{L}{4\pi\sigma}} \tag{8.10}$$

and so if a star is 100 times more luminous, then it is 10 times larger than another of the same temperature.
Larger, more massive early type stars are typically less dense than smaller stars.

Morgan–Keenan Luminosity Classes

Class	Type of Star
Ia-O	Extreme, luminous supergiants
Ia	Luminous supergiants
Ib	Less luminous supergiants
II	Bright giants
III	Normal giants
IV	Subgiants
V	Main-sequence (dwarf) stars
VI, sd	Subdwarfs
D	White dwarfs

Table 8.3: Morgan–Keenan Luminosity Classes

A luminosity class, designated by a Roman numeral, is appended to a star's Harvard spectral type. The numeral "I" (divided into subclasses Ia and Ib) is reserved for supergiant stars, and "V" is for the main sequence (with higher numerals for less luminous stars).
The ratio of the strengths of two closely spectral lines is often employed to place a star in the appropriate luminosity class. In general for stars of the same spectral type, narrower lines are usually produced by more luminous stars.

Subdwarfs (class IV) reside slightly to the left of the main sequences.
The M–K system doesn't extend to white dwarfs, who are designated the classification D.
The two-dimensional M–K classification allows distance calculation from a star's apparent magnitude and its vertical position on the HR diagram. The intrinsic scatter of about ± 1 magnitude for a specific luminosity class renders d uncertain by a factor of about $10^{1/5} \simeq 1.6$.

9.2 - Stellar Opacity

A star's spectra deviates substantially from the shape of the blackbody Planck function because stellar absorption lines remove light from a star's continuous spectrum at certain wavelengths. The decrease in intensity, produced by the dense series of metallic absorption lines, in the stellar spectrum is called line blanketing.

Temperature and Local Thermodynamic Equilibrium

There are many different measures of temperature within a star, defined according to the physical process being described:

- **Effective Temperature**, obtained from the Stefan-Boltzmann law

- **Excitation Temperature**, defined by the Boltzmann equation
- **Ionization Temperature**, defined by the Saha equation
- **Kinetic Temperature**, contained in the Maxwell-Boltzmann distribution
- **Colour Temperature** obtained by fitting the shape of a star's continuous spectrum to the Planck function

Although defined differently, the excitation, ionization, kinetic and colour temperatures are the same for a simple case of a gas contained within an "ideal box" in thermodynamic equilibrium. A star cannot be in thermodynamic equilibrium, however, due to the net outward flow of energy. That said, local regions of a star can be approximated as being in local thermodynamic equilibrium where particles and photons cannot escape the local environment and so are confined to an approximate "box" of nearly constant temperature.

The Definition of Opacity

Consider beams of parallel light rays travelling through a gas. Any process that removes photons from a beam of light will be collectively termed absorption. In this sense, scattering of photons is classed as absorption, as are energy level transitions (in sufficiently cool gases).
The change in intensity, dI_λ, of a ray of wavelength λ as it travels through a gas is proportional to its intensity, I_λ, the distance travelled, ds, and the density of the gas, ρ, by

$$\boxed{dI_\lambda = -\kappa_\lambda \rho I_\lambda \, ds} \tag{9.13}$$

where κ_λ is called the absorption coefficient, or **opacity**, and is wavelength dependent.
Define ℓ as the mean free path between atomic collisions as

$$\ell = \frac{1}{n\sigma} \tag{9.12}$$

where n is the number of atoms per cubic meter and σ is the collision cross-section of a particular atom: $\sigma = 4\pi a_0^2$ (a_0 atomic radius).
Now, define the characteristic distance of a photon as its "mean free path" by

$$\ell = \frac{1}{\kappa_\lambda \rho}$$

where ρ is the density of the medium through which the photon is travelling.
The intensity of a light beam falls by a factor of e^{-1} over this distance. Photospheric photons don't observed a constant temperature in stellar atmospheres, so local thermodynamic equilibrium doesn't apply.

Optical Depth

The mean free path is different for photons of different wavelengths. Both $\kappa_\lambda \rho$ and $n\sigma_\lambda$ can be thought of as the fraction of photons scattered per meter of distance.
It is convenient to define optical depth, τ_λ, back along a light ray as

$$\boxed{d\tau_\lambda = -\kappa_\lambda \rho ds} \tag{9.15}$$

where s is the distance measured along the photon's path in its direction of motion.

It's useful to think of optical depth as the number of mean free paths a light beam travels to the surface of some medium. Typically, we see no further than $\tau_\lambda \simeq 1$ into an atmosphere.
If $\tau_\lambda \gg 1$ through a medium, the gas is said to be optically thick. Conversely, if $\tau_\lambda \ll 1$ then the gas is said to be optically thin. As an example, Earth's atmosphere is optically thin.
Define $\tau_\lambda = 0$ at the surface of some medium. With this,

$$\tau_\lambda = \int_0^s \kappa_\lambda \rho ds \tag{9.17}$$

for some photon travelling s distance through an atmosphere. For the case of pure absorption, the decline in intensity of a ray of light that has travelled from an optical depth τ is

$$I_\lambda = I_{\lambda,0} e^{-\tau_\lambda} \tag{9.18}$$

where $I_{\lambda,0}$ is the initial intensity on emission.

General Sources of Opacity

In general, there are four sources of opacity. Each involves the change in the quantum state of an electron, and the terms bound and free are used to describe whether an electron is bound to an atom or ion in its initial and final states.

Bound-Bound Transitions occur when an electron makes a transition from one orbital to another. Thus, $\kappa_{\lambda,bb}$, the bound-bound opacity, is responsible for the absorption lines in stellar spectra. If a photon is absorbed and reemitted, it is essentially scattered. If it stays absorbed, it contributes to the thermal energy.

Bound-Free Absorption occurs when an incident photon ionizes an atom. Bound-free absorption, $\kappa_{\lambda,bf}$, is a contributor to the continuum opacity.

Free-Free Absorption is a scattering process that takes place when a free electron close to an ion absorbs a photon. It then emits a photon in a random direction. Free-free opacity, $\kappa_{\lambda,ff}$, is a contributor to the continuum opacity.

Electron Scattering involves a photon being scattered through Thomson scattering by a nearby free electron. Electron density must be very high, so it is dominant in hot stars and the interiors of stars where gases are mainly ionized. In high-temperature regimes, electron scattering dominates the continuum opacity, κ_{es}. A photon may also be scattered by an atomic electron if it is loosely bound to the nucleus. This is Compton scattering if $\lambda \ll$ the atom, or Rayleigh scattering if $\lambda \gg$ the atom.

9.3 - Radiative Transfer

In an equilibrium, steady-state star, there can be no change in the total energy contained within any one layer of the stellar atmosphere or interior. That is, absorption and emission energy must be in balance.

Photon Emission Processes

Any process that adds photons to a beam of light will now on be referred to as emission. Thus, emission includes scattering of photons *into* a beam, as well as electron-down transitions. In a star, there is not a direct flow of photons streaming towards the surface but rather a 'random walk' that eventually released energy from a star.

The Random Walk

As photons diffuse upwards through the stellar material, they follow a haphazard path called a random walk. The displacement that a photon travels is dependent on its mean free path and number of randomly directed steps, N, by

$$d = \ell\sqrt{N} \tag{9.29}$$

Therefore, it takes $N = n^2$ steps to travel n times the mean free path. The average number of steps needed for a photon to travel the distance d before leaving the surface is then

$$N = \tau_\lambda^2 \tag{9.30}$$

The average level in the atmosphere from which photons escape from is at a characteristic optical depth of about $\tau_\lambda = 2/3$. Therefore, a star's photosphere is defined as the layer from which its visible light originates: an optical depth of $\tau_\lambda \simeq 2/3$.
An observer will not see as deeply into the star at wavelengths where the opacity is greater than average. The intensity of radiation at $\tau_\lambda \simeq 2/3$ will decline the most for wavelengths where the opacity is greatest, resulting in absorption of lines in the visible spectrum.
Temperature must decrease outward for the formation of absorption lines (since only bound electrons can absorb energy).

Limb Darkening

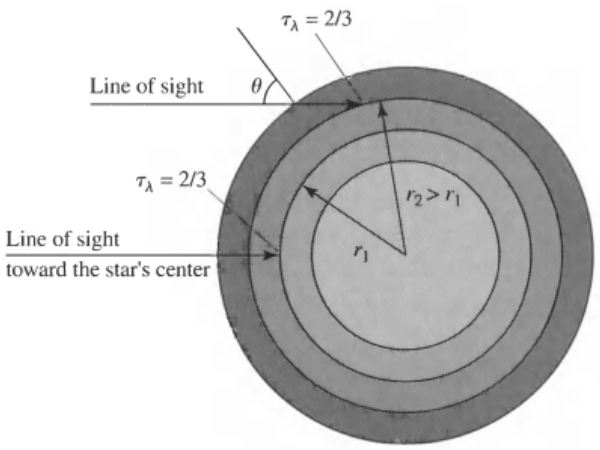

Looking near the limb (outer edge) of a star, an observer will not see as deeply into the stellar atmosphere and will therefore see a lower temperature at an optical depth of $\tau_\lambda \simeq 2/3$ (compared to looking perpendicular to the surface). As a result, a star appears darker (more red) on the rim than in the center.

Figure 9.12: Limb Darkening

6 Week 6 - Stellar Structure and Energy

10.1 - Hydrostatic Equilibrium

Stellar evolution is the result of a constant fight against the pull of gravity.

The Derivation of the Hydrostatic Equilibrium Equation

If we assume that a star is static,

$$\boxed{\frac{dP}{dr} = -G\frac{M_r\rho}{r^2} = -\rho g} \tag{10.6}$$

where $g \equiv \frac{GM_r}{r^2}$ is the local acceleration of gravity at the radius r in the star, and ρ is the local average density. Equation 10.6 is the condition for hydrostatic equilibrium, and is one of the fundamental equations of stellar structure for spherically symmetric objects. It clearly indicates that a pressure gradient must exist to counteract the force of gravity. This pressure increases as radius decreases.

The Equation of Mass Conservation

For a spherically symmetric star, consider a shell of mass M_r and thickness dr, located at a distance r from the center. Assuming that the shell is sufficiently thin ($dr \ll r$),

$$\boxed{\frac{dM_r}{dr} = 4\pi r^2\rho} \tag{10.7}$$

where ρ is the *local* density.

10.2 - Pressure Equation of State

An equation of state relates the dependence of pressure on other fundamental parameters of the material.

The Ideal Gas Law in Terms of the Mean Molecular Weight

Define the mean molecular weight as

$$\mu = \frac{\bar{m}}{m_H}$$

where $\bar{m}$ is the average mass of a particle in the medium, and m_H is the hydrogen mass. The mean molecular weight is just the average mass (as a multiple of the hydrogen mass) of a free particle in a gas.
The ideal gas law in terms of the mean molecular weight is

$$\boxed{P_g = \frac{\rho k T}{\mu m_H}} \tag{10.11}$$

For a neutral gas,

$$\frac{1}{\mu_n} \simeq X + \frac{1}{4}Y + \left\langle \frac{1}{A} \right\rangle_n Z \tag{10.14}$$

and for a completely ionized gas,

$$\frac{1}{\mu_i} \simeq 2X + \frac{3}{4}Y + \left\langle \frac{1+z}{A} \right\rangle_i Z \tag{10.16}$$

where A is the number of hydrogen masses a particle is, z is the number of free electrons, and $\{X, Y, Z\}$ correspond to the mass fractions of hydrogen, helium and metals.

The Contribution of Radiation Pressure

Because photons possess momentum, they are capable of delivering an impulse to other particles: another form of pressure. The radiation pressure is

$$\boxed{P_{\text{rad}} = \frac{1}{3}aT^4} \tag{10.19}$$

where a is the radiation constant $a = 4\sigma/c$.
Combining both the ideal gas and radiation pressure terms, the total pressure is

$$\boxed{P_t = \frac{\rho k T}{\mu m_H} + \frac{1}{3}aT^4} \tag{10.20}$$

10.3 - Stellar Energy Sources

Gravitation and the Kelvin-Helmholtz Timescale

Approximating ρ as its average value across a whole star, the gravitational potential energy, and consequently its total mechanical energy (by the Virial Theorem) are

$$U_g \sim -\frac{16\pi^2}{15} G \bar{\rho}^2 R^5 \sim -\frac{3}{5}\frac{GM^2}{R} \tag{10.22}$$

$$E \sim -\frac{3}{10}\frac{GM^2}{R} \tag{10.23}$$

The Kelvin-Helmholtz timescale, t_{KH}, describes the lifetime of a star by its current luminosity and energy liberation by gravitational collapse by

$$t_{\text{KH}} = \frac{\Delta E_g}{L} \simeq -\frac{E_f}{L} = \frac{3}{10}\frac{GM^2}{RL} \tag{10.24}$$

This estimates the Sun's lifetime as $t_{\text{KH}} \sim 10^7$ years, which clearly isn't right as the Earth is on the order of 10^9 years old. Therefore, gravitational potential energy alone cannot account for the Sun's luminosity throughout it's entire lifetime.

The Nuclear Timescale

The nucleus of an element is specified by its number of protons, Z. An isotope of an element is defined by its number of neutrons, N. Collectively, protons and neutrons are referred to as nucleons, with the number of nucleons in an isotope being $A = N + Z$.

A is a good indicator of the mass of an isotope, and is often referred to as the mass number. The masses of nucleons and electrons are

$$m_p \simeq 1.6726 \times 10^{-27} \text{ kg} \simeq 1.0072765\text{u}$$
$$m_n \simeq 1.6749 \times 10^{-27} \text{ kg} \simeq 1.0086649\text{u}$$
$$m_e \simeq 9.1094 \times 10^{-31} \text{ kg} \simeq 0.0005486\text{u}$$

where u is 1/12 the mass of Carbon-12: u$\simeq 1.66054 \times 10^{-27}$ kg.
Note that $m_p + m_e < m_H$. Since mass is equivalent to energy, and energy must be conserved, any loss in energy when an electron and proton combine to form an atom must come at the expense of lost mass. Similarly, energy is also released with an accompanying loss of mass when nucleons are combined to form atomic nuclei.

A He nucleus is 2 protons and 2 neutrons, created by 4H $\rightarrow$ He. This is a fusion reaction, where lighter particles fuse to form a heavier one. The combined mass of 4H exceeds that of 1He by about 0.7%, $\Delta m = 0.028697$u. Therefore, the total energy released in forming a helium nucleus is $\Delta E_b = \Delta m c^2 = 26.731$ MeV, which is known as the binding energy of He.
The nuclear timescale is defined as the lifetime of a star should its power come from nuclear reactions, and is given by

$$t_{\text{nuclear}} = \frac{E_{\text{nuclear}}}{L} = \frac{f \Delta e \cdot M c^2}{L} \tag{10.25}$$

where f is the fraction of a star undergoing fusion, Δe is the fraction of mass converted to energy, and M the mass of the star.
For the Sun, with $f = 0.1$ and $\Delta e = 0.07$, the nuclear time scale is $t_{\text{nuclear}} \sim 10^{10}$ years, which is more than enough time to account for the age of the solar system.

Quantum Mechanical Tunneling

Classical physics predicts the temperature required to sustain fusion as $\sim 10^{10}$K, but the Sun's core is on the order of $\sim 10^7$K. Quantum mechanical tunneling can explain the discrepancy.
Due to the uncertainty principle, particles can overcome repulsive intermolecular forces from tunneling their position (when their momentum, or equivalently thermal energy, is well defined). As a crude estimate, assume that a proton must be within one de Broglie wavelength to tunnel. Classical physics inaccurately predicts the temperature required for fusion as

$$T_{\text{classical}} = \frac{Z_1 Z_2 e^2}{6\pi\epsilon_0 k r} \tag{10.26}$$

while the quantum mechanical estimate of the temperature is

$$T_{\text{quantum}} = \frac{Z_1^2 Z_2^2 e^4 \mu_m}{12\pi^2 \epsilon_0^2 h^2 k} \tag{10.27}$$

where $Z_{1,2}$ are the number of protons in the nuclei of some fusing atoms 1 and 2 respectively. Assuming the collision of two protons, $\mu_m = m_p/2$, $Z_1 = Z_2 = 1$ and so $T_{\text{quantum}} \sim 10^7$K, which is consistent with the estimated temperature of the interior of the Sun.

First Proton-Proton Chains and the CNO Cycle

Smaller mass stars, with the lower temperature cores, are dominated by pp chains during the "hydrogen burning" evolution. More massive stars with correspondingly higher core temperature covert hydrogen to helium through the CNO cycle. The transition between reactions occur in stars slightly heavier than the Sun.

One chain of reactions that convert hydrogen to helium is the first proton-proton chain (PPI). The slowest step in all of the proton-proton chains is the first one, which involves two protons decaying into neutrons via the weak nuclear force.
A second, independent cycle exists for the production of helium-4. In the CNO cycle, carbon, nitrogen, and oxygen are used as catalysts and are consumed and regenerated in the process. This process is much more temperature dependent, hence why it mainly happens in higher mass stars.
When 4H $\rightarrow$ He, the mean molecular weight of the star increases. The ideal gas law predicts that the pressure will

then decrease. As a result, the star is no longer in hydrostatic equilibrium and will begin to collapse, which in turn raises the temperature and density to compensate. When temperature and density become sufficiently high, helium nuclei can overcome Coulomb repulsion and begin to burn.

The Binding Energy Per Nucleon

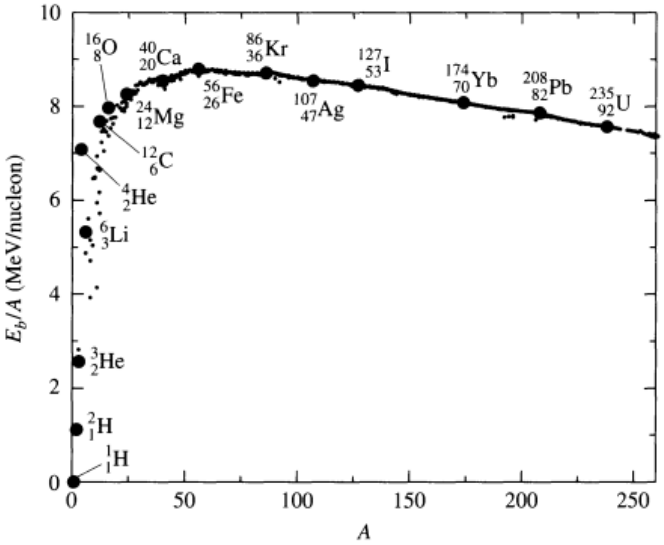

Figure 10.9: The Binding Energy per Nucleon

The binding energy per nucleon, E_b/A, is useful in understanding the energy release in fusion, where

$$E_b = \Delta mc^2 = [Zm_p + (A - Z)m_n - m_{\text{nucleus}}]\, c^2$$

The derivative of the curve of E_b/A vs A hints at the energy release of fusion for that element, where $^{5}6_{2}6\text{Fe}$ lies at the root of that derivative (or the turning point of Figure 10.9). When E_b/A reaches its peak, the gravitational forces in the star begin to outweigh fusion forces, since that star begins to lose energy from fusion reactions and cannot counteract gravitational collapse.

Figure 10.9 clearly shows that the fusion of 4 hydrogen nuclei into one helium-4 nuclei liberates the most energy – hence why the majority of the lifetime of *all* stars is spent fusing hydrogen.

The Luminosity Gradient Equation

Let ϵ be the total energy released per kilogram per second by all nuclear reactions and by gravity. The interior luminosity gradient, as a function of radius, is

$$\boxed{\frac{dL_r}{dr} = 4\pi r^2 \rho \epsilon} \tag{10.36}$$

where ρ is the average density over r.

11.1 - The Solar Interior

The Solar Neutrino Problem

All nuclear reactions produce neutrinos as a byproduct and is an efficient method of energy release of a star. The neutrinos produced in a star's core change before they reach a detector (on their escape through the star).
Fusion produces electron neutrinos (ν_e), however two other flavours also exist; the muon neutrino (ν_μ) and the tau neutrino (ν_τ).
Electron neutrinos interact with electrons on the journey out of a star's core, and oscillate between the aforementioned types.

7 Week 7 - Stellar Models and Formation

10.4 - Energy Transport and Thermodynamics

Three Energy Transport Mechanisms

Radiation allows the energy produced by nuclear reactions and gravitation to be carried to the surface via photons. The opacity of the medium plays an important role.
Convection involves hot, buoyant mass elements carrying excess energy outward while cool elements fall inward.
Conduction transports heat via molecular collisions, but is generally insignificant in stellar environments.

The Radiative Temperature Gradient

The temperature gradient for radiative energy transport is

$$\boxed{\frac{dT}{dr} = -\frac{3}{4ac}\frac{\bar{\kappa}\rho}{T^3}\frac{L_r}{4\pi r^2}} \tag{10.68}$$

where $\bar{\kappa}$ is the Rosseland Mean Opacity, and a is related to the radiation pressure gradient.
If the opacity or flux increase, the temperature gradient gets steeper.

The Pressure Scale Height

If the temperature gradient becomes too steep, convection can become significant. The timescale for convection, taken to be the amount of time required for a convective element to travel a characteristic distance, is in some cases approximately equal to the timescale for changes in the structure of the star. This implies that convection is strongly coupled to the star's dynamic behaviour.
The pressure scale height H_P, the distance over which the gas pressure decreases by a factor of e, is given by

$$H_P = \frac{P}{\rho g} \tag{10.70}$$

10.6 - The Main Sequence

The observational characteristic of a star must change as a consequence of the central nuclear reactions. If changes in the core are slow, so are evolutionary changes in observed surface features.

The Eddington Luminosity Limit

The stability of very massive stars is directly affected by their extremely high luminosities. Radiation pressure can dominate even in the outer regions of high mass stars. $L_{\rm ed}$ is the maximum radiative luminosity a star can have while remaining in hydrostatic equilibrium:

$$\boxed{L_{\rm ed} = \frac{4\pi G c}{\bar{\kappa}} M} \tag{10.114}$$

If the luminosity exceeds this, radiation pressure induced mass loss must occur. This is the Eddington Limit.
The close correspondence between theoretical and Eddington luminosities for high mass stars implies their outer envelopes are loosely bound. Observations of $\sim 100 M_\odot$ stars indicate significant mass loss and luminosity variability.

Variations of Main-Sequence Stellar Parameters with Mass

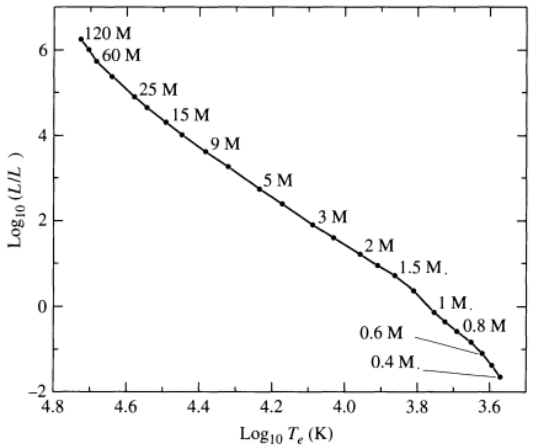

Figure 10.13: Locations of Stellar Models on a Theoretical HR Diagram

Stars undergoing hydrogen burning in their cores lie along the observational main sequence. Main sequence lifetimes decreases non-linearly with increasing luminosity.
The upper portion of the main sequence has convection dominated cores.

Near $1.2\mathrm{M}_\odot$, the pp-chain becomes dominant and the core primarily radiative. For stars of mass $< 1.3\mathrm{M}_\odot$, convection is more efficient than radiation near the surface. Entire stars are convective at around $\leq 0.3\mathrm{M}_\odot$.

12.1 - Interstellar Dust and Gas

The Interstellar Medium

Stars are born out of gas and dust that exist between the stars, known as the interstellar medium (ISM). Much of the star's material returns to the ISM through stellar wind and explosive events.

Interstellar Extinction

Interstellar extinction refers to the obscuration of stars (from an observer's perspective) due to the gas/dust clouds in the ISM, primarily due to scattering and absorption of starlight. The apparent magnitude with respect to the interstellar extinction A_λ is

$$m_\lambda = M_\lambda + 5\log_{10} d - 5 + A_\lambda \tag{12.1}$$

where $A_\lambda > 0$ is the number of magnitudes of interstellar extinction present, with $A_\lambda = 1.086\tau_\lambda$.
Hence, the change in magnitude due to extinction is approximately equal to the optical depth along the line of sight.

The Mie Theory

Since blue light is scattered more than red light, starlight passing through intervening dust clouds becomes reddened as blue light is removed. This causes stars to appear redder than their effective temperatures would imply.
As a result of blue light scattering, looking at the cloud in a direction other than the line of sight to a bright star will result in a blue reflection nebula.

The Classification of Interstellar Clouds

Diffuse Molecular Clouds (or Translucent Molecular Clouds) Typically have temperatures from 15K to 50K, mass from $3 \sim 100\mathrm{M}_\odot$ and measure several parsec across. Both H1 and and diffuse clouds tend to be irregularly shaped. Interstellar extinction usually $1 < A_\lambda < 5$.

Giant Molecular Clouds (GMCs) Temperatures typically ∼15K, $M \sim 10^5\mathrm{M}_\odot$, or up to $10^6\mathrm{M}_\odot$ and typically size on the order of 50pc across. Tend to be clumpy with local regions of significantly greater density.

- **Dark Cloud Complexes** are regions of GMCs with about $A_V \sim 5$, $M \sim 10^4\mathrm{M}_\odot$, and diameters on the order of 10pc.
- **Clumps** are smaller and more dense than dark cloud complexes, with $A_V \sim 10$, $M \sim 30\mathrm{M}_\odot$, $T \sim 10$K, and diameters of a couple of parsec.
- **Dense Cores** are smaller and denser than clumps, $A_V > 10$, $M \sim 10\mathrm{M}_\odot$, $T = 10$K and diameters of 0.1pc.

Hot Cores are possible regions of recent star formation, since they usually have young O or B class stars in their center. They have $A_V \sim 50$, $M \sim 10$ to $3000\mathrm{M}_\odot$, $T \sim 100 - 300\mathrm{K}$, and diameters of about 0.05 to 0.1pc.

Bok Globules are almost spherical in shape, and located outside larger molecular complexes. $A_V \sim 10$, $T \sim 10\mathrm{K}$, $M \sim 1 - 1000\mathrm{M}_\odot$, and sizes $\leq 1\mathrm{pc}$. They are usually sites of star formation for young, low–luminosity stars.

12.2 - The Formation of Protostars

The Jeans Criterion

Protostars are pre-nuclear burning objects, freshly formed from gas clouds. The minimum mass of a gas cloud needed to initiate spontaneous collapse, M_c, is related to the Jeans mass, M_J, by $M_c > M_J$ which is the Jeans Criterion. The **Jeans mass** is given by

$$\boxed{M_J \simeq \left(\frac{5kT}{G\mu m_H}\right)^{3/2}\left(\frac{3}{4\pi\rho_0}\right)^{1/2}} \tag{12.14}$$

The Jeans criterion may also be expressed in terms of the minimum radius needed to collapse a cloud of density ρ_0: $R_c > R_J$, where the **Jeans length** is

$$\boxed{R_J \simeq \left(\frac{15kT}{4\pi G\mu m_H \rho_0}\right)^{1/2}} \tag{12.16}$$

The critical mass required for gravitational collapse in the presence of an external gas pressure (surrounding ISM) of P_0 is given by the Bonnor-Ebert mass,

$$M_{\mathrm{BE}} = \frac{c_{\mathrm{BE}} v_T^4}{P_0^{1/2} G^{3/2}} \tag{12.17}$$

where $v_T \equiv \sqrt{kT/\mu m_H}$ is the isothermal sound speed, and $c_{\mathrm{BE}} \simeq 1.18$ is a dimensionless constant.

Homologous Collapse

Once gravitational collapse of a molecular cloud has begun, it is characterised by a free-fall timescale given by

$$t_{ff} = \sqrt{\frac{3\pi}{32}\frac{1}{G\rho_0}} \tag{12.26}$$

12.3 - Pre-Main-Sequence Evolution

Curves that depict the life histories of stars on the HR diagram are known as **evolutionary tracks**.

The Hayashi Track

As the temperature of the forming protostar increases, the opacity of the outer layers becomes dominated by the H^- ion. The large opacity contribution reduces the efficiency of radiation, and so the outer envelope of the star becomes convective. Due to the constraints that convection puts on the structure of a star, a deep convective envelope limits its quasi-static evolutionary path to a nearly-vertical line on a HR diagram.
As the collapse slows, luminosity decreases while temperature increases slightly. This is the **Hayashi Track**.

The Hayashi Track represents a boundary between "allowed" hydrostatic stellar models and those that are "forbidden". No stable stars can exist to the right of the Hayashi Track on a HR diagram. To the left of the Hayashi Track, convection/radiation are responsible for energy transfer. Collapsing gas clouds are on the right of the track, while main-sequence/giants are on the left.

Initial Mass ($M_\odot$)	Contraction Time (Myr)
60	0.0282
25	0.0708
15	0.117
9	0.288
5	1.15
3	7.24
2	23.4
1.5	35.4
1	38.9
0.8	68.4

Table 12.1: Pre-Main-Sequence Contraction Times

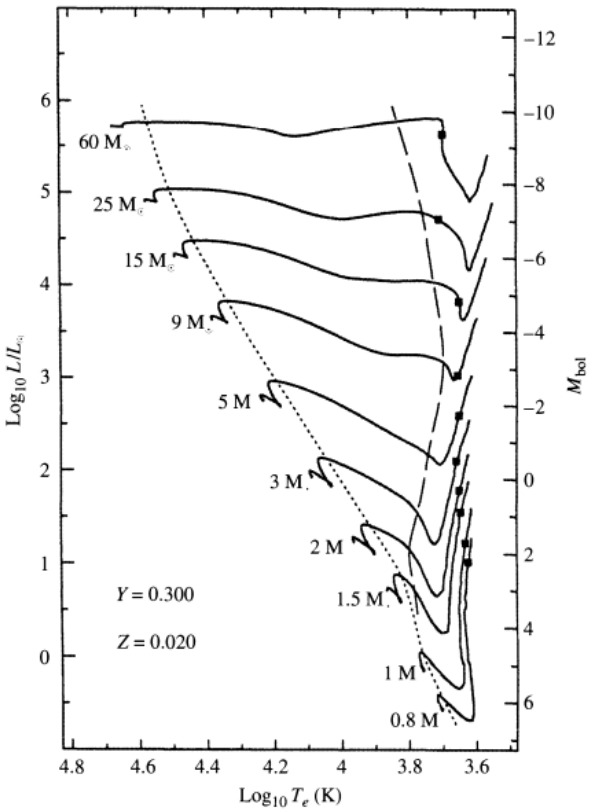

Figure 12.11: Classical Pre-Main-Sequence Evolutionary Tracks

The Zero-Age Main-Sequence (ZAMS)

The diagonal line in the HR diagram where stars first reach the main sequence and begin equilibrium hydrogen burning (Figure 12.11) is called the zero-age main sequence. The amount of time required for stars to collapse onto the ZAMS is inversely related to the mass as seen in Table 12.1.

8 Week 8 - Planetary Systems

23.1 - Characteristics of Extrasolar Planetary Systems

Mass Distribution of Extrasolar Planets

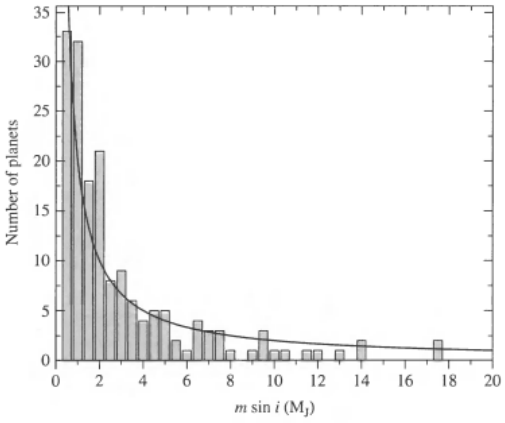

Figure 23.3: The Number of planets in mass bins of interval $0.5M_J$

Initially, the radial velocity technique was only able to discover very massive planets (on the order of M_J) in close orbits around their parent stars, partly due to these objects having the most significant reflex radial velocity effect, and partly due to their low periodicity (so that change was quickly apparent). Over time, this selection effect is systematically diminishing. When binned by mass interval, the number of planets in each mass bin varies as

$$\frac{dN}{dM} \propto M^{-1} \tag{23.1}$$

The Distribution of Orbital Eccentricities

Planets orbiting close to their parent star tend to have (mostly) circularized orbits. From data up to 2006, two conclusions were drawn:

1. Planets with orbital periods less than 5 days tend to have the smallest eccentricities (80% having $e < 0.1$), and
2. Planets sufficiently far from the parent star may have fairly large eccentricities, but still typically less than 0.5.

The Trend toward High Metallicity

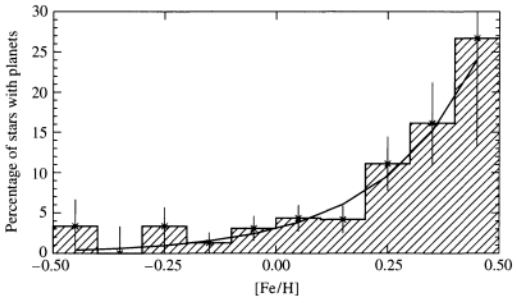

Figure 23.5: The percentage of stars found to have planetary systems, relative to the star's metallicity bin

It appears that there is a strong tendency for planetary systems to preferentially form around metal-rich stars. One way to quantify the **metallicity** is by comparing the rations of iron to hydrogen in stars relative to our sun:

$$[\text{Fe/H}] \equiv \log_{10}\left[\frac{(N_{\text{Fe}}/N_{\text{H}})_{\text{star}}}{(N_{\text{Fe}}/N_{\text{H}})_{\odot}}\right] \tag{23.2}$$

where N_{Fe} and N_{H} represent the *number* of iron and hydrogen atoms respectively. Stars with [Fe/H] < 0 are metal-poor relative to the Sun, and [Fe/H] > 0 metal-rich. Extremely metal-poor (population II) stars in the Milky Way have been measured with [Fe/H] values as low as -5.4, while the highest values for metal-rich (population I) stars are about 0.6.

According to the sample of 1040 F, G, and K stars used in some study, the data seems well fit by

$$\mathcal{P} = 0.03 \times 10^{2.0[\text{Fe/H}]} \tag{23.3}$$

where $\mathcal{P}$ is the probability of a star having a detectable planetary system.

Distinguishing Extrasolar Planets from Brown Dwarfs

Two different criteria have been proposed to distinguish a planet from a brown dwarf:

1. A proposed definition of a planet is that it is an object formed through a process beginning with the bottom-up accretion of planetesimals, whereas a brown dwarf forms directly from gravitational collapse.

2. The second proposed criterion is based on whether or not the object that forms is massive enough to ever have had nuclear fusion occur in its core. Computer models suggest that an object with $m \geq 13M_J$ could burn deuterium while forming. As an upper bound, stars with a mass of $0.072M_\odot$ ($75M_J$) undergo nuclear fusion at a sufficient rate to place them at the low-mass end of the main-sequence. Thus the criterion states that a brown dwarf's mass be $13M_J < M_{bd} < 75M_J$.

The latter criterion is generally accepted, due to the former being very difficult to determine.

23.2 - Planetary System Formation and Evolution

Accretion Disks and Debris Disks

Due to the associated angular momentum of a gas cloud, the gravitational collapse of said cloud leads to the formation of an **accretion disk**. There is growing evidence that clumps of material exist in these disks.
There is also substantial evidence of **debris disks** around older stars. The implication is that material is left over in the disk after the star has finished forming, which may be the extrasolar analogs to the asteroid and Kuiper belts.

Angular Momentum Distribution in the Solar System

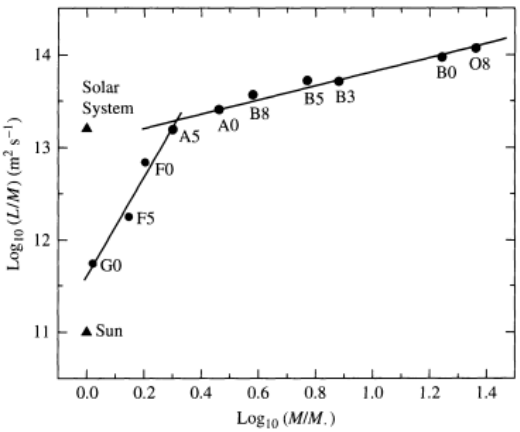

Figure 23.8: The average amount of angular momentum per unit mass as a function of mass for stars on the main sequence.

On average, main-sequence stars that are more massive rotate much more rapidly and contain more angular momentum per unit mass than do less massive stars.

The discrepancy in the angular momentum of the Sun compared to other stars (note that the Sun is G2) could be explained by mass loss by solar wind, and charged particles being trapped in the protosun's magnetic field and dragged as the Sun moved through space.

The change in slope of the angular-momentum-per-unit-mass curve responds well with the onset of surface convection in low-mass stars, which in turn is linked to the development of coronae and mass loss.

The Temperature Gradient in the Solar Nebula

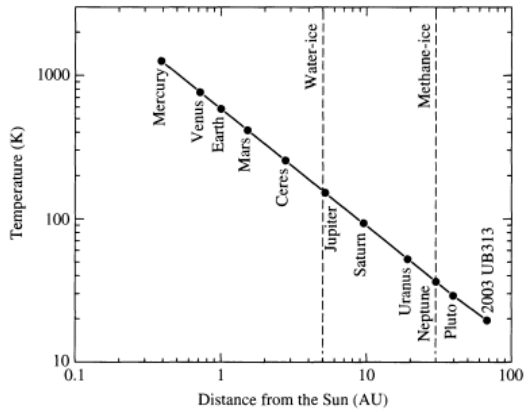

Figure 23.9: An equilibrium model of the temperature structure of the early solar nebula.

Either a composition gradient or a temperature gradient (or both) must have existed in the early solar nebula to describe the difference in planet composition with orbital radius. The volatile-poor inner planets and the volatile-rich outer (gas/ice) giant planets can be suitably explained by a temperature gradient in the early protosun accretion disk.
To an extent, temperature gradients describe the difference in moon composition. For example Jupiter's outer moons are more icy than the inner ones, suggesting that Jupiter's formation disk (subnebula) had its own temperature gradient.

Consequences of Heavy Bombardment

The present-day orientations for the spin axes of planets are notably inconsistent, particularly Mercury, Venus and Uranus. The only likely mechanism suggested to date that can naturally account for the range of orientations observed requires collisions of planets or protoplanets with large planetesimals.

The Gravitational Instability Formation Mechanism

One mechanism for planet formation is the idea that planets could form in accretion disks in a manner analogous to star formation, with self-collapse of local regions of a larger accretion disk producing planetesimals. This mechanism could even result in a local subnebula accretion disk forming around the protoplanet that could lead to the production of moons.
While this mechanism is attractive due to simplicity, simulations suggest that the solar nebula's lifetime would not have been sufficient to allow Uranus and Neptune to grow quickly enough to attain their respective masses. It also doesn't account for the mass distribution of extrasolar planets or the wide range in densities and core sizes of planets.

The Accretion Formation Mechanism

An alternative, more favoured model, is that planets grow from the "bottom up" through a process of accretion of smaller building blocks.

The Hill Radius

Within the nebular disk, small grains with icy mantles were able to collide and stick together randomly. When objects of appreciable size were able to develop in the disk, they began to gravitationally influence other material in their areas.
Define the **Hill radius**, R_H, to be the distance from the planetesimal where the orbital period of a test particle around the planetesimal is equal to the orbital period of the planetesimal around the Sun,

$$\boxed{R_H = \left(\frac{M}{M_\odot}\right)^{1/3} a} \tag{23.4}$$

where M is the mass of the planetesimal, and a is it's semi-major axis around the Sun.
The physical significance of the Hill radius is that if a particle comes within about one Hill radius of a planetesimal with a sufficiently low relative velocity, the particle can become gravitationally bound to the planetesimal.

The Process of Migration

Type I migration is proportional to mass, implying that as a planet accretes more material, it moves more rapidly towards its parent star. As the growing planet moves through the solar nebula, it continually encounters fresh material to "feed on". If a planet remained in a fixed orbit, it would quickly consume all of the available gas within a few Hill radii and only slowly grow after that. Migration instead allows it to move through the disk without creating a significant gap in the nebula.

Type II migration causes slowly orbiting particles farther out to speed up because of collisions with higher-velocity particles occupying slightly smaller orbits. The loss of kinetic energy by the inner particles causes them to spiral inward. Type II migration can become more the significant (but slower) migration process when a gap is opened up in the disk.

Outward migration is also possible via the scattering of planetesimals inward which results in migration outward.

Resonance Effects in the Early Solar System

When the orbital resonance of Jupiter and Saturn reached a 2:1 resonance, their gravitational influence on the smaller bodies in the solar system combined, causing significant perturbations to the smaller objects. It's likely that this resonance (occurring roughly 700Myr after formation - due to migration) caused the heavy bombardment in the solar system.

9 Week 9 - Stellar Evolution, Star Clusters and Asteroseismology

13.1 - Evolution on the Main Sequence

Low-Mass Main-Sequence Evolution

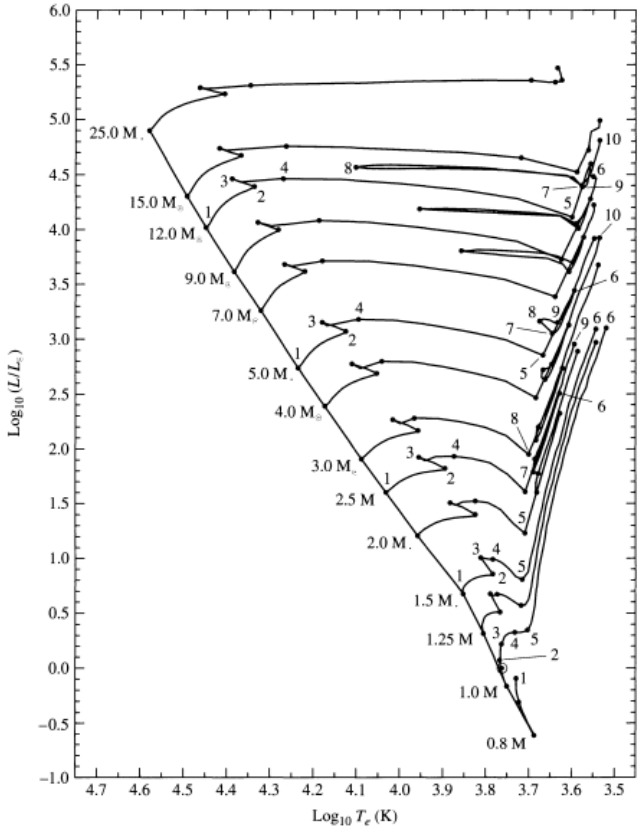

Figure 13.1: Main Sequence and Post-Main-Sequence Evolutionary Tracks of Stars with X=0.68, Y=0.30, and Z=0.02

As low mass stars fuse hydrogen in their cores, the mean molecular weight decreases and the the star slightly collapses. In response, the temperatures increase slightly to maintain pressure.
Once all of the core hydrogen is depleted, energy generation from the pp chain must stop (in the core) leaving a helium 'ash' core, with a thick hydrogen-burning shell around the core producing energy. At this point, the luminosity being generated in the shell actually exceeds what was produced by the core during the main sequence. As a result, the star begins to move vertically on the HR-diagram (see point 3 for a Solar mass star). Some of the energy produced in this phase goes to slowly increasing the radius of both the star and hydrogen-burning shell. Consequently, the star's temperature decreases slightly, and the evolutionary track bends to the right (lower temperature).

Worth noting is that the small (mostly) helium core contributes next to nothing in terms of luminosity, and comprises about 3% of the stars mass. It is isothermal, and so a density gradient results in the necessary pressure gradient to support the weight of the star above.

The Schonberg-Chandrasekhar Limit

The above mentioned phase of evolution ends when the mass of the isothermal core becomes too great and the core is no longer capable of supporting the mass above it. The maximum fraction of a star's mass that can exist in an isothermal core and still support the above layers is

$$\boxed{\left(\frac{M_{ic}}{M}\right)_{SC} \approx 0.37\left(\frac{\mu_{\rm env}}{\mu_{ic}}\right)^2} \tag{13.1}$$

where $\mu_{\rm env}$ and μ_{ic} are the mean molecular weights of the overlying envelope and isothermal core respectively. When the mass of the isothermal helium core exceeds this limit, the core collapses on a Kelvin-Helmholtz timescale, the star evolving very rapidly as a result. This corresponds to point 4 on Figure 13.1 for a Solar mass star.

Main-Sequence Evolution of Massive Stars

The evolution of more massive stars on the main sequence is similar to that of lower-mass stars with a notable difference: the existence of a convective core. This convection continually mixes material, thereby keeping the core composition essentially homogeneous. This applies since the timescale for convection (defined by the amount of

time taken for a convective element to travel one mixing length [see sec 10.4]) is much shorter than the nuclear timescale. For a $5M_\odot$ star, the central convection zone decreases somewhat during core hydrogen burning, leaving behind a slight composition gradient. Higher mass stars experience the central convection zone deteriorating more rapidly, up to a point at around $10M_\odot$ where the central convection zone disappears entirely before hydrogen is exhausted.

When the mass fraction of hydrogen reaches about $X = 0.05$ in the core of a $5M_\odot$ star, the entire star begins to contract. The release of some gravitational potential energy results in the luminosity increasing, the radius decreases and the temperature increasing. For stars above $1.2M_\odot$, this signals the end of the main sequence.

13.2 - Late Stages of Stellar Evolution

Evolution Off the Main-Sequence

The late-stage evolution is somewhat different for a $5M_\odot$ star, where the entire star contracts slightly on the Kelvin-Helmholtz timescale (seen by jumps between points 2 and 3 on Figure 13.1). At about point 3 on the graph, the temperature increases to a point where hydrogen can once again fuse in a shell around the core.

The Subgiant Branch

The process of gravitational energy release on the KH timescale results in the expansion of the star and temperature cooling. This phase is known as the subgiant branch (SGB).
As the core collapses, a temperature gradient is re-established and the temperature and density of the hydrogen-burning shell increases. The shell narrows significantly and energy output increases rapidly. The stellar envelope then expands, absorbing some of the produced energy in the process (and reducing luminosity as a result [see point 5 in Figure 13.1]).

The Red Giant Branch

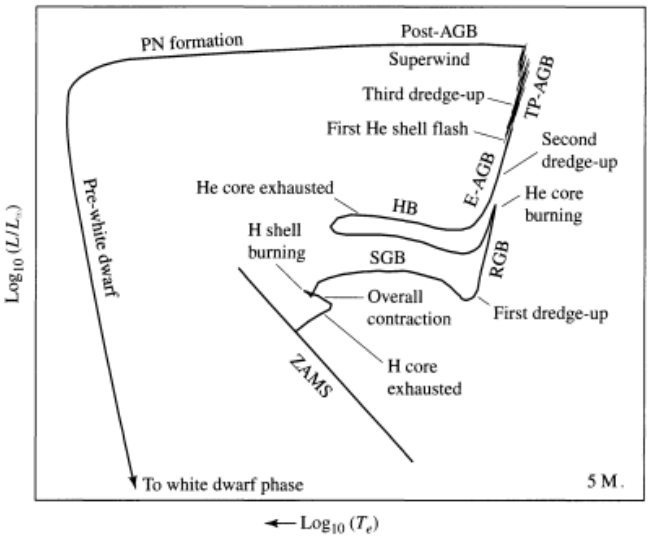

Figure 13.5: Diagram of the Evolution of an Intermediate Mass Star

With the expansion of the stellar envelope and decrease in effective temperature, the photospheric opacity increases. This results in a convection zone developing near the surface for both low and intermediate mass stars. As the star continues to evolve to point 5 in Fig 13.1, the convection zone penetrates deeper into the star providing more efficient energy transport. The result is the luminosity shooting far upward in a similar line to the Hayashi track - a phase called the red giant branch (RGB).
As the star climbs the RGB, the convection zone deepens into areas of chemical composition having been affected by nuclear processes. The convection currents then transport ${}^{3}_{2}\mathrm{He}$ and ${}^{14}_{7}\mathrm{N}$ outward, and ${}^{12}_{6}\mathrm{C}$ inward. This transport of materials from the deep interior to the surface is referred to as the **first dredge-up** phase.

The Red Giant Tip

At the tip of the RGB (point 6 in Fig 13.1), central temperature and density finally become high enough for quantum mechanical tunneling to become effective at fusing helium nuclei. With this new energy, the core expands and the hydrogen burning shell cools due to being pushed outwards. The rate of energy production in the shell decreases and the total star's luminosity abruptly decreases - causing the envelope to contract and increase in temperature.

The Helium Core Flash

In low mass stars ($\leq 1.8M_\odot$) towards the end of the RGB phase, the core temperatures and pressures *eventually* reach a point where the triple alpha process of helium fusion begins. Due to neutrinos effectively transferring energy out of the centre of the star, the central temperature is actually less than just outside the core, and the triple alpha process begins in a shell around the core first. This ignition of helium, produces a lot of energy very quickly and soon the entire core begins the process, lifting the temperature inversion. The resulting production of energy is on the order of $10^{11}L_\odot$ - comparable to that of an entire galaxy, if only for a few seconds. Most of the energy doesn't reach the surface, and is instead absorbed by much of the stellar envelope causing some mass to be lost from the exterior. This process is referred to as the **helium core flash**.

The Horizontal Branch

Following the red giant tip, the increasing compression on the hydrogen-burning shell eventually causes the energy output of the shell (and so the energy output of the star) to begin to rise again. With the increase in temperature, the deep convection zone in the envelope rises to the surface while at the same time, a convective core develops (due to the high temperature dependence of the triple alpha process). This blueward evolution is referred to as the **horizontal branch** (HB) loop.
When the star reaches its most blueward point (Fig 13.1, point 8), the mean molecular weight of the core increases so much that the core begins to contract, and the envelope expands and cools. Shortly after this, the core helium is exhausted and the star progresses redward rapidly. The increase in core temperature corresponds to a thick helium burning shell surrounding the CO core. As the core shrinks more, the helium shell narrows and strengthens, forcing material above to expand and cool further, which temporarily "shuts off" the hydrogen-burning shell.
During the HB passage, many stars develop instabilities and fluctuate in luminosity, temperature and radius.

The Early Asymptotic Giant Branch

When the redward evolution of the horizontal branch reaches the Hayashi track, the evolutionary track bends upward along a path called the asymptotic giant branch (AGB). During this phase, the helium-burning shell dominates the energy output of the star, and the expanding envelope absorbs much of the energy produced thereby expanding and cooling more. The convective currents deepen once more from the hydrogen rich envelope to the helium-rich region above the He-burning shell. The material transported to the surface and mixed corresponds to the **second dredge-up**, which increases helium and nitrogen content in the envelope.

The Thermal-Pulse Asymptotic Giant Branch

Near the upper portion of the AGB, the dormant hydrogen-burning shell eventually reignites and dominates the energy output of the star. During this phase, the narrowing helium-burning shell begins to turn off and on quasi-periodically. These intermittent **helium shell flashes** occur due to helium ash (from the hydrogen-burning shell above) falling onto the helium layer and igniting fusion. This drives the hydrogen shell outward, cooling it and "turning it off" again. This process repeats for some time.
The period between pulses is a function of the stellar mass, ranging from thousands of years for $5M_\odot$ to hundreds of thousands of years for $0.6M_\odot$, with the pulse amplitude growing in each successive case.

A class of pulsating variable stars known as **long-period variables** (LPVs) are in fact AGB stars with pulsation periods of 100 to 700 days.

Third Dredge-Up and Carbon Stars

Due to the sudden energy flux from helium-burning flashes, convection zones are established between the helium-burning shell and the hydrogen-burning shell. For massive enough stars (above $2M_\odot$), the convection zones of the star will merge and extend into regions where carbon has been created. During this third dredge-up phase, carbon rich material is brought to the surface, decreasing the ratio of oxygen to carbon. If there are multiple third-dredge-up events, the oxygen-rich spectrum of a star will transform into a carbon-rich spectrum.
Carbon stars are designated with a C spectral type, and show carbon rich spectra. Intermediate between M and C spectral types are the **S spectral type** stars, which have almost equal proportions of carbon and oxygen in their atmospheres.

Mass Loss and AGB Evolution

AGB stars lose mass at a rapid rate by **superwind**, as much as a 10 thousandth of a solar mass per year, and have quite cool effective temperatures of about 3000K. As a result, dust grains form in the expelled matter - silicate grains for oxygen-rich environments, and granite grains in carbon-rich environments. For stars of less than a mass of about $4M_\odot$, the CO core will never ignite nuclear burning, and these stars appear to be shrouded in optically thick dust clouds that radiate energy primarily through the infrared.

Post-Asymptotic Giant Branch

As the cloud around the star continues to expand, it eventually becomes optically thin and exposes the star of an F or G supergiant spectrum. At this point, the star is heading horizontally across the HR diagram blueward as a **post-AGB** star. During this final phase of mass loss, the remainder of the star's envelope is expelled leaving only a very thin layer of material above the burning-shells - extinguishing them. The luminosity drops rapidly, and the hot central object will cool to become a **white dwarf star**.

Planetary Nebulae

The expanding shell of gas around a white dwarf progenitor is called a planetary nebula. These nebulae owe their appearance to UV light emitted by the central 'star', exciting or ionising the gaseous atoms which emit visible light when relaxed.
After only about 50000 years, a planetary nebula will dissipate into the ISM.

13.3 - Stellar Clusters

Population I, II, and III Stars

The first stars to form after the Big Bang had virtually no metallicity, $Z = 0$. The next generation that formed from their ejected material and the ISM were extremely **metal-poor**, having very low but non-zero Z. Each successive generation resulted in higher Z, leading to metal rich stars with Z as high as 0.03. This first stars are referred to as **Population III**, metal-poor stars with $Z \gtrsim 0$ are **Population II**, and metal rich stars **Population I**. Population I stars are generally found in the galactic disk, while Population II stars can be found well above and below the disk.

Globular Clusters and Open Clusters

Every member of a given cluster formed from the same cloud, with essentially identical compositions and within a similar period of time. The Vogt-Russell theorem suggests that the differences in evolutionary states between the stars in a cluster are solely due to their initial masses. Population II stars tend to be in globular clusters, formed when the Milky Way was young. Population I clusters tend to be smaller and younger, called open clusters.

Spectroscopic Parallax

Since the dimensions of a cluster are usually small compared to that of the distance that they are away, HR diagrams can be constructed of the cluster's stars using the apparent magnitude instead of the absolute magnitude. By matching the *observational* main sequence against a main sequence calibrated in absolute magnitude, the distance modulus of the cluster can be determined (alternatively referred to as **main-sequence fitting**).

14.1 - Stellar Pulsation

Pulsating stars dim and brighten periodically as their surfaces expand and contract. Pulsating stars can vary on the order of thousands of years, to just days and seconds, and stars similar to δ Cephei, **classical Cepheids**, are vital to astronomy.

The Period-Luminosity Relation

The luminosity (and thus the absolute magnitude) of a variable star is intrinsically related to the period of its pulsation.

The observed period-luminosity relation in the V band is described by

$$\boxed{M_{\langle V\rangle} = -2.81 \log_{10} P_d - 1.43} \tag{14.1}$$

where $M_{\langle V\rangle}$ is the average absolute V magnitude, and P_d is the pulsation period in days. The accuracy can be substantially increased by observing in the infrared (where interstellar extinction isn't as prevalent), where the infrared period-luminosity fit is

$$\boxed{H = -3.234 \log_{10} P_d + 16.079} \tag{14.3}$$

14.2 - The Physics of Stellar Pulsation

The Period-Density Relation

The radial oscillations of a pulsating star are the result of sound waves resonating in the star's interior. A rough estimate of the pulsation period, Π, is

$$\boxed{\Pi \approx \sqrt{\frac{3\pi}{2\gamma G\rho}}} \tag{14.6}$$

where ρ is the approximated *constant* density and γ is the "adiabatic gamma".

14.4 - Nonradial Stellar Pulsation

As some types of stars pulsate, their surfaces do not move uniformly in and out, but by a more complicated nonradial motion in which some regions of the surface expand while others contract.

The p and f Modes

In section 14.2, the radial pulsation of stars was attributed to standing sound waves in the stellar interior. For nonradial oscillations, sound waves can propagate horizontally as well as radially to produce waves that travel around the star. Because *pressure* provides the restoring force for sound waves, these nonradial oscillations are called **p modes**.
f modes can be thought of as a surface gravity wave, with a rise in amplitude with radius.

The g Modes

Just as pressure supplies the restoring force for the compression and expansion of p-mode sound waves, *gravity* is the source of the restoring force for nonradial oscillations called g-modes, which are produced by internal gravity waves. These waves involve a "sloshing" back and forth of stellar gases, which is connected to the buoyancy of stellar material.

14.5 - Helioseismology and Asteroseismology

The Five-Minute Solar Oscillations

The oscillations observed on the Sun have modes with periods between three and 8 minutes, and very short horizontal wavelengths. The five-minute p-modes (3.33 mHz) are concentrated below the photosphere within the Sun's convection zone.

δ Scuti Stars and Rapidly Oscillating Ap Stars

Asteroseismology is the study of pulsation modes of stars in order to investigate their internal structures and characteristics.

10 Week 10 - Close Binary Systems

18.1 - Gravity in a Close Binary System

If binary stars are very close, then one or both stars may have their outer layers gravitationally deformed into a teardrop shape. As a star rotates through the tidal bulge raised by its partner's gravitationally pull, it is forced to pulsate. Orbital and rotational energy is dissipated in this way until the system reaches the state of minimum energy resulting in synchronous rotation (tidal locking) and circular orbits.

Lagrangian Points and Equipotential Surfaces

The effective gravitational potential at any point in orbit around a binary is

$$\boxed{\Phi = -G\left(\frac{M_1}{s_1} + \frac{M_2}{s_2}\right) - \frac{1}{2}\omega^2 r^2} \tag{18.4}$$

where s_1 and s_2 are the distances of an object to the primary and secondary masses respectively, r_1 and r_2 are the distances of the masses from the centre of mass, r is the distance of the object from the centre of mass, and ω is the angular frequency of the objects orbit.

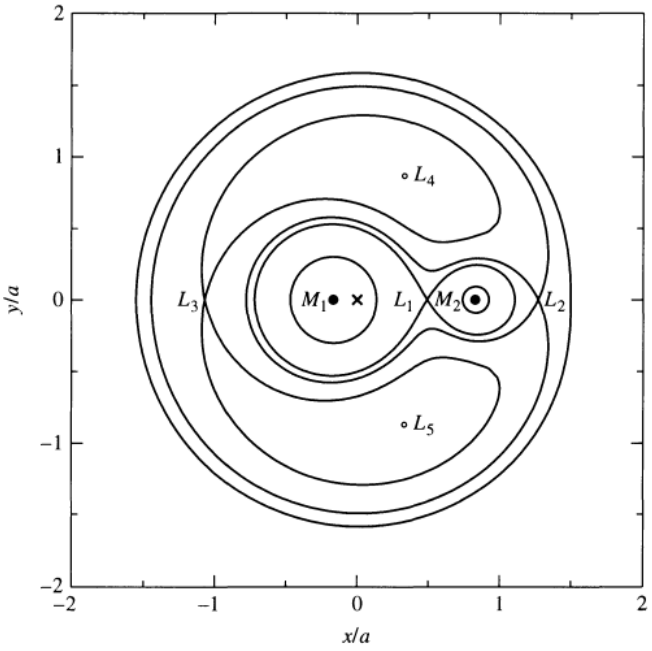

Lagrangian Points are points in the effective gravitational potential where there is no net force on a test mass (i.e. the differential of the potential is zero with respect to distance).
Lagrangian points 1, 2, and 3 are *unstable* points as they are local maxima of Φ. Points 4 and 5 are *stable*, as they lie at a trough of Φ. Intuitively, some perturbation of a test mass at points 1-3 will destabilise a test mass and remove it from the lagrange point, accelerating it away from the equilibrium position. A perturbation of a mass at points 4 or 5 will cause it to oscillate about the lagrange point (in a kidney bean shape).
It's clear from Figure 18.3 that close to the masses M_1 or M_2, the equipotential contours are nearly spherical due to the gravity from that mass dominating the region. As either star evolves, it will expand to 'fill' the equipotential contours.

Figure 18.3: Equipotentials where $M_1 > M_2$

Classes of Binary Star Systems

The appearance of a binary system depends on which equipotential surfaces are filled by the stars. A **detached binary** describes a binary system in which the stars evolve nearly independently.
If one star expands enough to fill the "figure-eight" contour, then it's atmospheric gases can escape through the L_1 point towards its companion. The teardrop shaped regions of space bounded by this equipotential surface are called **Roche lobes**. When the transfer of mass between stars begins after one star has expanded through its Roche lobe, the system is called a **semidetached binary**. The star that fills the lobe and loses mass is usually called the **secondary star** with mass M_2, and the companion the **primary star** with mass M_1.

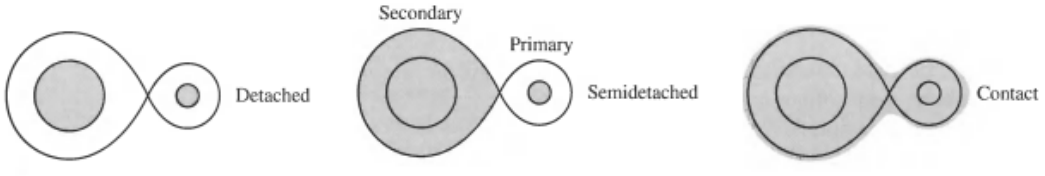

Figure 18.4: Classification of Binary Star Systems

It may happen that both stars fill or expand beyond their Roche lobes. In this case, the two stars share a common atmosphere bounded by a dumbbell-shaped equipotential surface (such as the one passing through L_2 in Fig 18.3). This is a **contact binary**.

Mass Transfer Rate

The *rough* mass transfer rate for a semidetached binary is

$$\dot{M} \simeq \pi R \rho d \sqrt{\frac{3kT}{m_H}} \tag{18.14}$$

where R is the radius of the secondary star, ρ its density, T its temperature and d the distance of 'overlap' between the two stars.

11 Week 11 - White Dwarfs and Accretion Disks

16.1 - The Discovery of Sirius B

Sirius B, a white dwarf companion to the A0 star Sirius, was inferred by angular velocity measurements (by Bessel, 1838) with a periodicity of its orbit of about 50 years. In 1862, it was finally observed only due to the the stars being at their apastrons relative to each other (separated by just 10"), and was impossible to be observed earlier due to their relative brightness ($L_A = 23.5L_\odot$ and $L_B = 0.03L_\odot$) and close proximity to each other.
At the next apastron 50 years later, scientists measured the surface temperatures of each star and found that Sirius B was incredibly hot, on the order of 27000K. Stefan-Boltzmann's law implied that the size of Sirius B is only $0.008R_\odot$ - smaller than Earth with a full Solar mass.

16.2 - White Dwarfs

White dwarfs have approximately the mass of the Sun and are the size of the Earth. Only a few have been characterised sufficiently due to their faintness.

Classes of White Dwarf Stars

White dwarfs occupy a narrow sliver of the HR diagram that is roughly parallel to and below the main sequence. The name itself is a misnomer as they have surface temperatures (colours) ranging from 80000K to 5000K.
White dwarfs are characterised by the D ("dwarf") spectral type, with the largest group (about 2/3 of the total population) being **DA white dwarfs** that display only pressure-broadened hydrogen absorption lines in their spectra. Hydrogen lines are absent from **DB white dwarfs** (8% - which show only helium absorption) and **DC white dwarfs** (14% - which show no absorption at all). The remaining types are **DQ white dwarfs** which exhibit carbon features in their spectra, and **DZ white dwarfs** that show evidence of metal lines.

Central Conditions in White Dwarfs

For Sirius B at least, central pressures and temperatures can be estimated to be roughly $P_c \approx 3.8 \times 10^{22}$ N m^{-2} and $T_c \approx 7.6 \times 10^7$K respectively. This gives an interesting conclusion in that hydrogen can't be present (in appreciable amounts) below the surface layers of a white dwarf, less hydrogen fusion would occur and the white dwarf would be orders of magnitude more luminous than observed. So, white dwarf centres must be comprised of particles that are incapable of fusion at those temperatures and pressures − most white dwarfs consist primarily of completely ionized carbon and oxygen nuclei. The distribution of DA white dwarf masses is sharply peaked at $0.56M_\odot$, with about 80% lying between $\pm 0.14M_\odot$.

Spectra and Surface Composition

The exceptional pull of white dwarf gravity pulls the heavier nuclei inwards, leaving the lightest elements on the surface resulting in a thin outer layer of hydrogen covering a layer of helium on top of a carbon-oxygen core.

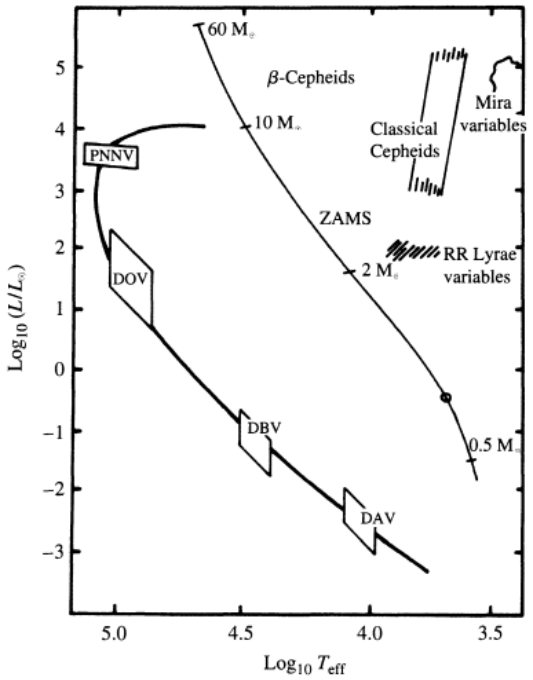

Figure 16.4: Compact Pulsators on the HR Diagram

Pulsating White Dwarfs

White dwarfs with temperatures of $T_e \approx 12000$K lie within the instability strip on the HR diagram and pulsate with periods between 100 and 1000s. These **ZZ Ceti** variables are variable DA white dwarfs, known also as **DAV stars**. The pulsation periods correspond to non-radial g-modes that involve almost perfectly horizontal displacements and so the radii of these compact pulsators hardly change. The brightness variations observed (typically a few tenths of a magnitude) are due to temperature variations on the surface.

Hydrogen partial ionization zones are responsible for driving the oscillations of ZZ Ceti stars, while hotter DB white dwarfs exhibit g-mode oscillations driven by the helium partial ionization zone, denoted **DBV** stars. The location of these are shown in Fig 16.4 along with **DOV** and **PNNV** ($T_e \approx 10^5$K) variables that are associated with the birth of white dwarfs ["PNN" stands for planetary nebula nuclei, and the DO spectral type marks the transition to the white dwarf stage].

All of these types have multiple periods, simultaneously showing at least 3 and as many as 125 different frequencies.

16.3 - The Physics of Degenerate Matter

The Pauli Exclusion Principle and Electron Degeneracy

Any system of particles consists of quantum states that are identified by a set of quantum numbers. If the particles are fermions (electrons, neutrons, etc), then the Pauli exclusion principle allows at most one fermion in each quantum state because no two fermions can have the same set of quantum numbers.

As energy is removed from a system, an increasingly large fraction of particles are forced into the lower energy states and since they are fermions, all of the particles cannot crowd into the ground state. Instead, the fermions will fill up the lowest available unoccupied states. Even in the limit $T \to 0$K, the motion of the fermions in excited states produces a pressure in the fermion gas. At zero temperature, all of the lower energy states and none of the higher energy states are occupied, and such a gas is completely **degenerate**.

The Condition for Degeneracy

At any temperature above absolute zero, some of the states with an energy less than ε_F (the Fermi energy, or the maximum energy of any electron in a completely degenerate gas) will become vacant as fermions use their thermal energy to occupy other, more energetic states. Although the degeneracy will not be precisely complete when $T > 0$K, the assumption of complete degeneracy is a good approximation for the densities encountered in the interior of a white dwarf - all but the most energetic particles will have an energy less than the Fermi energy. In rough terms, if the average thermal energy of an electron is less than the Fermi energy ($\frac{3}{2}kT < \varepsilon_F$), then an average electron will be unable to make a transition to an unoccupied state and the electron gas will be degenerate. The condition for degeneracy may be written as

$$\boxed{\frac{T}{\rho^{2/3}} < \mathcal{D}} \tag{16.6}$$

where $\mathcal{D} \equiv 1261$ K m^2 kg$^{-2/3}$ (for a medium with an equal number of protons and neutrons). The smaller the value of $T/p^{2/3}$, the more degenerate the gas.

Electron Degeneracy Pressure

Electron degeneracy pressure is the result of the Pauli exclusion principle and the Heisenberg uncertainty principle, where the small enclosed volume of electrons necessitates a large uncertainty (and thus magnitude) in its momenta. The pressure due to electron degeneracy is then

$$\boxed{P = \frac{(3\pi^2)^{2/3}}{5}\frac{\hbar^2}{m_e}\left[\left(\frac{Z}{A}\right)\frac{\rho}{m_H}\right]^{5/3}} \tag{16.12}$$

where Z/A is the ratio of protons to nucleons in the white dwarfs nuclei. Using $Z/A = 0.5$ for a carbon-oxygen white dwarf, the electron degeneracy pressure available to support a white dwarf such as Sirius B is about 1.9×10^{22} N m^{-2} - within a factor of two of the initial estimate for central pressure made previously. *Electron degeneracy pressure is responsible for maintaining hydrostatic equilibrium in a white dwarf.*

16.4 - The Chandrasekhar Limit

The requirement that a white dwarf is supported by electron degeneracy pressure implies that there is a maximum mass for white dwarfs.

The Mass-Volume Relation

The volume of a white dwarf is inversely proportional to its mass, so a more massive white dwarf is actually smaller. This **mass-volume relation** is a result of the star deriving its support from electron degeneracy pressure, and is described by

$$\boxed{M_{\rm wd}V_{\rm wd} = \text{constant}} \tag{16.14}$$

Intuitively, the electrons must be more closely confined to generate the larger degeneracy pressure required to support a more massive star. However, when accounting for relativistic effects, a massive white dwarf is actually *smaller* than predicted by the mass-volume relation. Zero volume occurs for a finite value of mass, implying that there is a limit to the amount of matter that can be supported by electron degeneracy pressure.

Dynamical Instability

In the nonrelativistic case ($M \ll M_{\rm Ch}$), the white dwarf is dynamically stable in that a small perturbation (some mass addition) will eventually stabilise and the star will return to its equilibrium structure. For the extreme relativistic limit (where electron speed $v \approx c$), the white dwarf becomes dynamically unstable and a small perturbation will result in core collapse as electron degeneracy fails.

Estimating the Chandrasekhar Limit

The Chandrasekhar limit, the theoretical maximal mass for a white dwarf, corresponds to $M_{\rm Ch} = 1.44$ M$_\odot$. No white dwarf has been discovered with a greater mass.
The pressure of a completely degenerate electron gas is independent of its temperature, which has the effect of decoupling mechanical structure of a star from its thermal properties. This decoupling results in the helium flash of ageing stars which ultimately results in a carbon-oxygen white dwarf. In cases where a star is not massive enough to facilitate helium burning, a helium white dwarf is ultimately formed.

16.5 - The Cooling of White Dwarfs

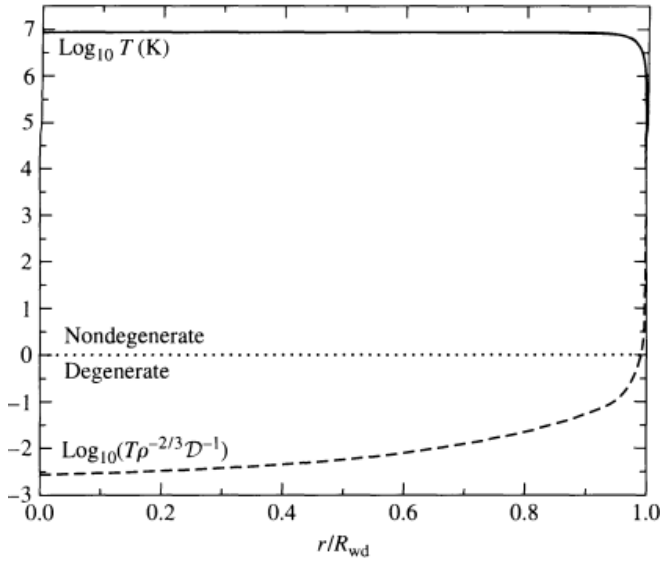

Figure 16.8: Temperature and Degree of Degeneracy wrt Radius in a White Dwarf

Energy Transport

In a white dwarf, energy is carried by **electron conduction** rather than by radiation, as degenerate electrons can travel long distances before losing energy in a collision with a nucleus. This is so efficient that the interior of a white dwarf is nearly isothermal, with the temperature dropping significantly only in the nondegenerate surface layers.

The steep temperature gradient near the surface creates convection zones that may alter the appearance of the white dwarf's spectrum as it cools.

The surface of a white dwarf cools more slowly than its isothermal interior as the star's thermal energy leaks into space.

The luminosity of a white dwarf is proportional to $T_c^{7/2}$ (the interior temperature).

The Cooling Timescale

The cooling timescale for a white dwarf is about 170 million years, and is an underestimate since the cooling timescale increases as T_c decreases. In reality, a white dwarf spends most of its life cooling slowly with a low temperature and luminosity.

Crystallization

As a white dwarf cools, the material in the centre begins crystallising in a process that gradually moves outward. As the cooling nuclei settle into a crystalline lattice (maintained by mutual electrostatic repulsion) their energy is minimised as they vibrate about their average position in the lattice. Eventually undergoing a phase change, their latent heat is released which slows the stars cooling for a period. As the temperature continues to drop, the crystalline lattice accelerates the cooling as the lattice structure promotes further energy loss, and so white dwarfs eventually die as a cold, carbon-oxygen crystal.

18.2 - Accretion Disks

If the radius of a primary star is less than about 5% of the binary separation a, the mass stream will miss striking the primary's surface and instead goes into orbit around the primary to form a thin **accretion disk** of hot gas in the orbital plane. **Viscosity**, an internal friction that converts the directed kinetic energy of bulk mass motion into random thermal motion, causes the orbiting gases to lose energy and slowly spiral inward toward the primary. The gas is heated throughout its descent to increasingly higher temperatures as the lost orbital energy is converted into thermal energy. Finally, the gas is deposited onto the surface of the primary.

The Temperature Profile and Luminosity

At each radial distance, an optically thick disk emits blackbody radiation with a continuous spectrum corresponding to the local disk temperature at that distance.

As the gas spirals inward, its total energy E becomes more negative and the lost energy maintains the disk's temperature and is ultimately emitted in the form of blackbody radiation.

The temperature of the accretion disk at some radius r from the centre of the primary (of mass M, radius R, and

mass accretion rate of $\dot{M}$) is

$$T = T_{\rm disk}\left(\frac{R}{r}\right)^{3/4}\left(1-\sqrt{R/r}\right)^{1/4}; \qquad T_{\rm disk} = \left(\frac{3GM\dot{M}}{8\pi\sigma R^3}\right)^{1/4} \tag{18.19 \& 18.20}$$

where $T_{\rm disk}$ is a characteristic temperature of the disk and is roughly twice the maximum disk temperature ($\times 0.488$) which occurs at $r = (49/36)R$. The luminosity of the disk is

$$L_{\rm disk} = G\,\frac{M\dot{M}}{2R} \tag{18.23}$$

The accretion disk radiates away half of the available accretion energy (the energy delivered by deposited matter on the primary star), leaving the other half to be deposited on the surface of the primary (or in the turbulent boundary layer between the rapidly rotating disk and slowly rotating star).

The Radial Extent of an Accretion Disk

A rough estimate of the outer radius of the accretion disk is $R_{\rm disk} \approx 2r_{\rm circ}$, where

$$r_{\rm circ} \simeq a\left[0.5 - 0.227\log_{10}\left(\frac{M_2}{M_1}\right)\right]^4\left(1+\frac{M_2}{M_1}\right) \tag{18.25}$$

where M_1 and M_2 correspond to the primary and secondary respectively. The value $r_{\rm circ}$ corresponds to the radius at which a continuous stream of mass passing through L_1 settles in a circular orbit (by colliding with itself and removing energy over multiple orbits).

18.3 - A Survey of Interacting Binary Systems

The life history of a close binary system is complicated due to the effects of a changing mass ratio (M_2/M_1) as matter transfers between the secondary and primary. As this changes, the distribution of angular momentum, the orbital period of the system, and even the separation of the stars all change which ultimately results in the change of extent of the Roche lobes.

The Effects of Mass Transfer

The rate of change of semi-major axis with respect to mass transfer between two stars is

$$\frac{1}{a}\frac{da}{dt} = 2\dot{M}_1\frac{M_1 - M_2}{M_1 M_2} \tag{18.28}$$

As orbital separation decreases, the angular frequency of the stars orbits increase.

The Evolution of a Binary System

The following illustrates the probable evolution of a binary system that is destined to become a cataclysmic variable.

1. Take a widely separated binary system of two main-sequence stars ($M_1 > M_2$) that have a periodicity of months to a few years.
2. Star 1 evolves more rapidly, progresses to a giant/supergiant and overfills its Roche lobe. Mass transfer between star 1 (the secondary) and star 2 (the primary) begins resulting in Eq 18.28 being negative (negative change in semi-major axis) and the stars spiraling closer together with a shorter period.
3. As a has decreased, the Roche lobe around star 1 shrinks and the mass transfer rate increases under the positive feedback. This produces an extended atmosphere around the two stars, and the system is now a contact binary with the degenerate core of star 1 and the main-sequence star 2 sharing a common gaseous envelope. The stars transfer angular momentum to this envelope and spiral in closer still.
    i. If the cores of the two stars merge, the result will be a single star (which could explain blue stragglers in stellar clusters.

ii. Alternatively, the envelope may be ejected leaving the system as a detached binary. This scenario will be considered going forward.

4. Star 2 (now a secondary) now lies within its Roche lobe and star 1 (now a primary) cools to become a white dwarf. Eventually, the originally less-massive secondary star evolves to fill its Roche lobe and mass flows in the opposite direction (with $\dot{M}_1 > 0$). In this case a negative feedback mitigates the transfer process, as Eq 18.28 implies the stars now spiral further apart. For mass-transfer to sustain, either the secondary must expand faster than the Roche lobe grows, or angular momentum of the system has to decrease by some other means (stellar winds interacting with magnetic fields or by gravitational radiation). For the sake of progression, a steady rate of mass transfer from the secondary to the primary will be considered for the remainder of the scenario.

5. As the secondary evolves, another common envelope stage occurs which is subsequently expelled. What is left are two carbon-oxygen white dwarfs in a very tight orbit, circling each other every 15-30 seconds. The larger white dwarf overflows its Roche lobe and dissolves into a heavy disk that is accreted by the more massive dwarf. The accretion pushes the primary to the Chandrasekhar limit, which then explodes as a Type Ia supernova.

Types of Interacting Binary Systems

The following list describes the *main* classes of interacting binaries.

Algols These are two normal stars (main-sequence or subgiants) in a semidetached binary system. These systems are important for studying accretion process, and the mass loss from Algols may contribute to the chemical enrichment of the interstellar medium.

RS Canum Venaticorum and **BY Draconis Stars** These stars are chromospherically active binaries that are important systems for investigating dynamo-driven magnetic activity in cool stars, and contribute to our understanding of magnetic activity of stars.

W Ursae Majoris Contact Systems These short period (0.2-0.8 day) contact binaries display very high levels of magnetic activity and are important for studying the stellar dynamo. The drag of magnetic breaking may cause these binaries to coalesce into single stars.

Cataclysmic Variables and **Nova-like Binaries** These systems have short periods and contain white dwarf components together with cool M-type secondaries that fill their Roche lobes.

X-ray Binaries with Neutron Star/Black Hole Components These systems are powerful X-ray sources due to the interaction of gas onto the degenerate component of the system from a nondegenerate companion.

ζ **Aurigae and VV Cephei Systems** These long-period interacting binaries contain a late-type supergiant component and a hot companion. Although not originally interacting binaries, they became so when the more massive star evolved to become a supergiant. When eclipses occur, the atmosphere and wind of the cooler supergiant can be probed as the hotter star passes behind.

Symbiotic Binaries Symbiotic stars are long-period interacting binaries consisting of an M giant and an accreting component that can be a white dwarf, subdwarf, or low-mass main-sequence star. The common feature of these systems is the accretion of the cool components wind onto its hot companion.

Barium and S-Star Binaries These stars are thought to be long-period binaries in which the originally more massive components evolved and transferred some of its nuclear-processed gas to the present K or M giant companion.

Post-Common-Envelope Binaries These binary systems usually contain hot white subdwarf components and cooler secondary stars that have presumably passed through the common-envelope phase of binary star evolution.

12 Week 12 - Supernovae, Neutron Stars and Pulsars

15.1 - Post-Main Sequence Evolution of Massive Stars

Luminous Blue Variables

The class of extremely luminous ($> 10^6 L_\odot$) blue variable stars are often referred to as **S Doradus variables, Hubble-Sandage variables**, and **luminous blue variables** (LBVs). Examples of such stars are η Carinae and P Cygni.
As a class, LBVs tend to have high effective temperatures of between 15000K and 30000K, with luminosities in excess of $10^6 L_\odot$. Given the composition of their atmospheres and ejecta, LBVs are clearly evolved, post-main-sequence stars which cluster in an instability region in the HR diagram, suggesting that their behaviour is transient and turning on shortly after leaving the main sequence (and subsequently ceasing after some period of time).
A few possible explanations for these stars involve :

1. A modification of the "classical" Eddington limit to include a temperature dependence, which corresponds to a radiation pressure dominating over gravity at the surface of LBVs, and thus, significant mass loss.
2. Atmospheric pulsations develop with large amplitudes, and high irregularity.
3. Possible binary companions influencing mass loss (*eta* Car has an observed periodicity of 5.54 years)
4. High rotation velocity of the stars, resulting in a lower effective gravity at the equator from centrifugal effects - making the equatorial gasses more likely to dissipate.

None of these explanations have been proven, however, and only exist as *possible* explanations.

Wolf-Rayet Stars

Closely related to LBVs are Wolf-Rayet stars (WR), with an estimated population of 1000-2000 in the Milky Way. They are characterised by very strong, very broad emission lines, effective temperatures between 25000K and 100000K, and mass loss rates in excess of 10^{-5} $M_\odot$ per year. There is strong evidence that they have wind speeds ranging from 800 to 3000 km/s, and equatorial rotation speeds of typically 300km/s.

Whereas LBVs are all very massive stars of $85M_\odot$ or more, WRs can have progenitor masses as low as $20M_\odot$, and do not demonstrate the dramatic variability characteristic of LBVs.
Today, three classes of WR stars are recognised:

WNs: The spectra of these stars are dominated by emission lines of helium and nitrogen, with detectable emission from C, O, and H in some WN stars.

WCs: The spectra exhibit emission lines of helium and carbon, with a distinct absence of nitrogen and hydrogen lines.

WOs: Much rarer than the other two classes, WOs have spectra containing prominent oxygen lines, with some contribution from highly ionized species.

The literature sub-classifies WN and WC stars based on the degree of ionization in their atmospheres, ranging from WN2 to WN9 (for "early" [more] and "late" [less] ionized respectively) and WC4 through WC9. For example, a highly ionized WC star would be referred to as a WCE star, and a somewhat ionized WC would be referred to as a WCL.
The trend in composition from WN to WC to WO is a direct consequence of mass loss. WNs have virtually all of their hydrogen-dominated envelopes, where convection in the core has brought equilibrium CNO cycle-processed material to the surface. Mass loss results in the ejection of the CNO processed material, exposing helium-burning material generated by the triple alpha process (WC star). Then, if the star survives long enough, the mass loss will eventually strip away all but the oxygen component of the triple-alpha ash (WO star).
In addition to LBVs and WRs, the upper portion of the HR diagram also contains **blue supergiant stars** (BSG), **red supergiant stars** (RSG), and **Of stars** (O supergiants with pronounced emission lines).

A General Evolutionary Scheme for Massive Stars

A general evolutionary path for massive stars has been outlined below, with each case ending with a **supernova** (SN).

$$
\begin{aligned}
M > 85\,\mathrm{M}_\odot &: \ \mathrm{O} \to \mathrm{Of} \to \mathrm{LBV} \to \mathrm{WN} \to \mathrm{WC} \to \mathrm{SN} \\
40\,\mathrm{M}_\odot < M < 85\,\mathrm{M}_\odot &: \ \mathrm{O} \to \mathrm{Of} \to \mathrm{WN} \to \mathrm{WC} \to \mathrm{SN} \\
25\,\mathrm{M}_\odot < M < 40\,\mathrm{M}_\odot &: \ \mathrm{O} \to \mathrm{RSG} \to \mathrm{WN} \to \mathrm{WC} \to \mathrm{SN} \\
20\,\mathrm{M}_\odot < M < 25\,\mathrm{M}_\odot &: \ \mathrm{O} \to \mathrm{RSG} \to \mathrm{WN} \to \mathrm{SN} \\
10\,\mathrm{M}_\odot < M < 20\,\mathrm{M}_\odot &: \ \mathrm{O} \to \mathrm{RSG} \to \mathrm{BSG} \to \mathrm{SN}
\end{aligned}
$$

The Humphreys-Davidson Luminosity Limit

The most massive stars never evolve into the red supergiant portion of the HR diagram from the scenario above, which is in agreement with observations. As such, there is an upper-luminosity cut-off in the HR diagram that includes a diagonal component running from the highest luminosities and effective temperatures to lower values in both parameters. When full redward evolutionary tracks develop for stars below about $40\mathrm{M}_\odot$, the Humphreys-Davidson luminosity limit continues at constant luminosity.

15.2 - The Classification of Supernovae

Classes of Supernovae

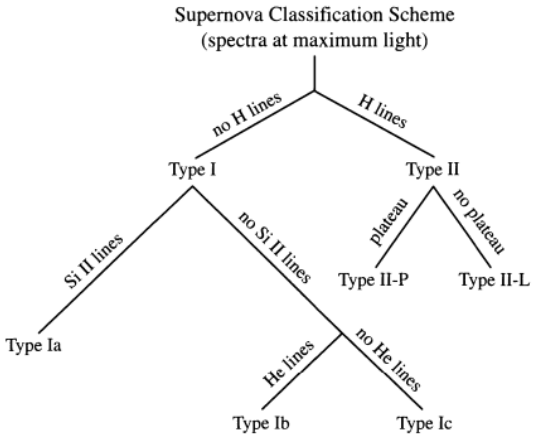

Figure 15.9: Classification of Supernovae

Type I supernovae were identified first as those supernovae that do not exhibit hydrogen lines in their spectra. They can be further subdivided into **Type Ia** (that show a strong Si II line at 615nm), and **Types Ib** and **Ic** based on the presence (Ib) or absence (Ic) of strong helium lines.

- Types Ib and Ic have only been observed in star forming regions of spiral galaxies (H II regions), which suggests that short-lived massive stars are probably involved.
- The typical peak brightness of a Type Ia is $M_B = -18.4$, while the light curves of Types Ib and Ic are fainter by 1.5 to 2 magnitudes in blue light (but are otherwise similar). All Type I supernovae show similar rates of decline of their brightness after maximum, about 0.065 ± 0.007 mag per day at 20 days, and after about 50 days the rate of dimming slows and becomes constant (with Type Ia declining 50% faster than the others).

Type II supernovae contain strong hydrogen lines, and are characterized by a rapid rise in luminosity that reaches a maximum brightness typically 1.5 mag dimmer than a Type Ia. Type II spectra also exhibit lines associated with heavier elements as well as hydrogen. The light curves of Type II are classified as either **Type II-P** (plateau) or **Type II-L** (linear). A temporary but clear plateau exists between about 30 and 80 days after maximum light for II-P supernovae, and Type II-P supernovae occur about 10 times as often as Type II-Ls do.

15.3 - Core-Collapse Supernovae

A typical Type II releases 10^{46}J of energy, with about 1% of that appearing as kinetic energy of the ejecta, and less than 0.01% being released as photons. The remainder of the energy is radiated in the form of neutrinos. Similar values are obtained for Type Ib and Ic supernovae.

Core-Collapse Supernova Mechanism

The very high temperature in the core of a massive star means that carbon and oxygen can burn towards the end of its life (in contrast to $M \leq 8\mathrm{M}_\odot$ stars where C and O is inert). Types II, Ib and Ic are known as **core-collapse**

supernovae.

As the helium-burning shell continues to add ash to the C-O core, eventually carbon burning is initiated which generates a variety of by-products, leading to a succession of nuclear reaction sequences (that depend sensitively on the mass of the star). Assuming that each reaction reaches equilibrium, an "onion-like" shell structure develops in the interior of the star. Following carbon burning, the oxygen in the neon-oxygen core will ignite producing a new core dominated by Si. At temperatures near 3×10^9K, silicon burning commences.
Silicon burning produces a host of nuclei centered near the $^{56}_{26}$Fe peak of the binding energy per nucleon curve (Fig 10.9), with any further reactions being endothermic which don't contribute to the luminosity of the star. As such, silicon burning is said to produce an *iron core*. Since burning of successively larger nuclei produces progressively less energy (per unit mass of fuel), the timescale for each succeeding reaction sequence becomes shorter.

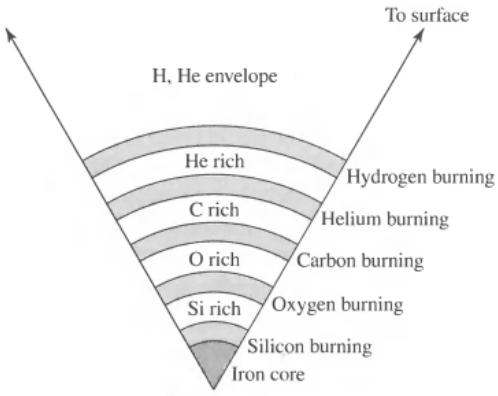

Figure 15.10: Shell Structure of a Massive Star

At the very high temperatures now present in the core, the photons possess enough energy to destroy heavy nuclei; a process known as **photodisintegration**. When the mass of the contracting iron core has become large enough and the temperature sufficiently high, photodisintegration destroys large nuclei in an extremely endothermic process that 'steals' energy away from supporting the star above the core against collapse. Under these extreme conditions, the free electrons that had assisted in supporting the star through degeneracy pressure are capture by heavy nuclei and by the protons that were produced through photodisintegration; for instance: $p^+ + e^- \rightarrow n + \nu_e$. The amount of energy that escapes in the form of neutrinos (by the above reaction) is enormous (several orders of magnitude higher than the photon luminosity).

Through these processes, most of the core's support in the form of electron degeneracy pressure is suddenly gone and the core begins to collapse extremely rapidly. In the inner portion of the core, the collapse is homologous and the velocity of the collapse is proportional to the distance away from the center of the star. At the radius where the velocity exceeds the local sound speed, the collapse can no longer remain homologous and the inner core decouples from the now supersonic outer core, which is left behind and nearly in free-fall. During the collapse, speeds can reach almost 70000km/s.

Since mechanical information propagates through the star at the speed of sound (slower than the core collapse), the outer layers (including the O, C, and He shells) are almost 'suspended' above the catastrophically collapsing core. The homologous collapse of the inner core continues until the density exceeds about 3 times atomic nuclei density, at which point the strong nuclear force (usually attractive) becomes repulsive. This results in the inner core rebounding somewhat, sending pressure waves outward into the infalling material. As the shock wave encounters the infalling outer iron core, the high temperatures that result cause further photodisintegration, robbing the shock of much of its energy (for every $0.1\mathrm{M}_\odot$ of broken down iron, the shock loses 1.7×10^{44}J). At this point, the shock stalls, with infalling matter accreting onto it. In other words, the shock has become an **accretion shock**, somewhat akin to the situation during protostellar collapse. Below the shock, a **neutrinosphere** develops from the processes of photodisintegration and electron capture. Some of the neutrino energy ($\approx 5\%$) will be deposited into the matter behind the shock as the matter is so dense that they cannot easily penetrate it. The additional energy heats the material and allows the shock to resume propagation towards the surface where the shock will drive the envelope and the remainder of the nuclear-processed matter in front of it. The total kinetic energy in the expanding material is on the order of 10^{44}J. Finally, when the material becomes optically thin at a radius of about 10^{13}m (≈ 100AU), a tremendous optical display results, releasing approximately 10^{42}J of photon energy, with a peak luminosity of nearly 10^{36}W, or roughly $10^9\mathrm{L}_\odot$, which is comparable to an entire galaxy.

The details that result in a Type II rather than a Ib or Ic have to do with the composition and mass of the envelope at the time of core collapse. Type II supernovae, which a more common than Ib or Ic, are usually red supergiant stars in the extreme upper-right-hand corner of the HR diagram at the time they undergo catastrophic core collapse. Type Ib's and Ic's have lost various amounts of their envelopes prior to detonation. Type Ib's and

Ic's may correspond to the detonation of WN and WC Wolf-Rayets, respectively.

Stellar Remnants of a Core-Collapse Supernova

If the initial mass of the star on the main sequence was not too large (perhaps $M_{\rm ZAMS} < 25{\rm M}_\odot$), the remnant in the inner core will stabilize and become a **neutron star** supported by neutron degeneracy pressure (a star sufficiently metal-rich may form a neutron star even if it's initial mass was much greater than $25{\rm M}_\odot$). However, if the initial stellar mass is much larger, even the pressure of neutron degeneracy cannot support the remnant against the pull of gravity and the final collapse will produce a **black hole**.

The Light Curves and the Radioactive Decay of the Ejecta

Type II-P supernovae are the most common type of core-collapse, supernova, and the source of the plateau in its light curve is due largely to the energy deposited by the shock into the hydrogen-rich envelope. The gas, which was ionized by the shock, enters a stage of prolonged recombination, releasing the energy at a nearly constant temperature of about 5000K.
The plateau may be further supported by the energy deposited by the **radioactive decay** of $^{56}_{28}$Ni that was produced by the shock front during its propagation through the star (along with other radioactive isotopes produced by explosive nucleosynthesis).
The energy released by the decay is deposited into the optically thick expanding shell, which is then radiated away from the supernova remnant's photosphere. This "holds up" the light curve for a time, extending the observed plateau. Eventually, the expanding gas cloud will become optically thin, exposing the central product of the explosion, be it a neutron star or black hole.

The number of remaining isotopes is related to the original population, N_0, the elapsed time, and the half-life of the isotope, $\tau_{1/2}$, by

$$\boxed{N(t) = N_0 e^{-\lambda t} \qquad \lambda = \frac{\ln 2}{\tau_{1/2}}} \tag{15.10}$$

Type II-L supernovae appear to have had progenitor stars with significantly reduced hydrogen envelopes, implying that the signature of the radioactive decay becomes evident almost immediately after the event.

s-Process and *r*-Process Nucleosynthesis

When nuclei having progressively higher numbers of protons, Z, form via stellar nucleosynthesis, it becomes increasingly difficult for other charged particles to react with them (due to a high Coulomb potential barrier). Since neutrons aren't charged, nuclear reactions involving *free* neutrons can occur even at relatively low temperatures. The reactions with neutrons result in more massive nuclei that are either stable or unstable against the beta-decay reaction (neutron decaying into a proton and by-products). If the beta-decay half-life is short compared to the timescale for neutron capture, the neutron-capture reaction is said to be a *slow process*, or an ***s*-process** reaction. *s*-Process reactions tend to yield stable nuclei.
On the other hand, if the half-life for the beta-decay reaction is long compared with the time scale for neutron capture, the neutron-capture reaction is termed a *rapid process*, or ***r*-process** and results in neutron-rich nuclei. *s*-Process reactions tend to occur in normal stellar evolution, while *r*-processes can occur during a supernova when a large flux of neutrinos exists. Although neither process plays significant roles in energy production, they do account for the abundance ratios of nuclei with $A > 60$ in the universe.

16.6 - Neutron Stars

Neutron Degeneracy

Because neutron stars are formed when the degenerate core of an aging supergiant star nears the Chandrasekhar limit and collapses, we take $M_{\rm Ch}$ for a typical neutron star mass. A 1.4 solar mass neutron star is essentially a huge nucleus with a mass number of $A \approx 10^{57}$ that is held together by gravity and supported by **neutron degeneracy pressure**. The expression for the estimated neutron star radius is

$$R_{\rm ns} \approx \frac{(18\pi)^{2/3}}{10} \frac{\hbar^2}{G M_{\rm ns}^{1/3}} \left(\frac{1}{m_H}\right)^{8/3} \tag{16.24}$$

The above formula is inaccurate by around a factor of 3 (the actual radii of neutron stars are around 3× larger).

The Density of a Neutron Star

A 1.4 solar mass neutron star would have an average density of 6.65×10^{17} kg/m$^3-$ about three times greater than the density of a typical atomic nucleus. In some sense, the neutrons must be "touching" one another. The pull of gravity at the surface of this 1.4 solar mass star (with $R = 10$km), is $g = 1.86 \times 10^{12}$m/s^2, or about 190 billion times Earth surface gravity.

Neutron Star Models

While the details are sensitive to the equation of state used, this model displays some typical features:

Transition density (kg m^{-3})	Composition	Degeneracy pressure
	iron nuclei, nonrelativistic free electrons	electron
$\approx 1 \times 10^9$	electrons become relativistic	
	iron nuclei, relativistic free electrons	electron
$\approx 1 \times 10^{12}$	neutronization	
	neutron-rich nuclei, relativistic free electrons	electron
$\approx 4 \times 10^{14}$	neutron drip	
	neutron-rich nuclei, free neutrons, relativistic free electrons	electron
$\approx 4 \times 10^{15}$	neutron degeneracy pressure dominates	
	neutron-rich nuclei, superfluid free neutrons, relativistic free electrons	neutron
$\approx 2 \times 10^{17}$	nuclei dissolve	
	superfluid free neutrons, superconducting free protons, relativistic free electrons	neutron
$\approx 4 \times 10^{17}$	pion production	
	superfluid free neutrons, superconducting free protons, relativistic free electrons, other elementary particles (pions, ...?)	neutron

Table 16.1: Composition of Neutron Star Material

- The outer crust consists of heavy nuclei, in the form of either a fluid "ocean" or solid lattice, and relativistic degenerate electrons. Nearest the surface, the nuclei are probably $^{56}_{26}$Fe. At greater depth and density, increasingly neutron-rich nuclei are encountered until neutron drip (free neutrons) begins at the bottom of the outer crust ($\rho \approx 4 \times 10^1 4$kg/m^3).
- The inner crust consists of a three-part mixture of a lattice of heavy nuclei, a superfluid of free neutrons (a fluid that doesn't experience viscosity), and relativistic degenerate electrons. The bottom of the inner crust occurs where $\rho \approx \rho_{\rm nuc}$ (nuclei density), and the nuclei dissolve.
- The interior of the neutron star consists primarily of superfluid neutrons, with a smaller number of superfluid, superconducting (zero electrical resistance) protons and relativistic degenerate electrons.
- There may or may not be a solid core consisting of pions or other sub-nuclear particles. The density at the center of a 1.4M$_\odot$ neutron star is about 10^{18}kg/m^3.

The Chandrasekhar Limit for Neutron Stars

Like white dwarfs, neutron stars obey a mass-volume relation:

$$\boxed{M_{\rm ns} V_{\rm ns} = \text{constant}} \tag{16.25}$$

so neutron stars become smaller and more dense with increasing mass. However, there exists a point at which neutron degeneracy pressure can no longer support the star, and so there is a maximum mass; 2.2M$_\odot$ for a static neutron star, and 2.9M$_\odot$ if it is rotating rapidly. If the neutron star's mass exceed this, it cannot provide pressure against a perturbation fast enough to avoid collapsing, and the end result is a black hole.

Rapid Rotation and Conservation of Angular Momentum

If the iron core of the pre-supernova supergiant star were rotating even slowly, the decrease in radius would be so great that the conservation of angular momentum would guarantee the formation of a rapidly rotating neutron star. Since the ratio of the iron core radius to the neutron star radius is about 512, this correlates to a period relation of

$$P_{\rm ns} \approx 3.8 \times 10^{-6}\ P_{\rm core} \tag{16.27}$$

The above is only an estimate, as the core rotation isn't entirely detached from the outer envelope as a result of magnetic/viscosity processes.
Neutron stars typically rotate on the order of a few milliseconds.

"Freezing In" Magnetic Field Lines

A property predicted for neutron stars was that they should have extreme magnetic fields. The "freezing in" of magnetic field lines in a conducting fluid or gas implies that the magnetic flux through the surface of a white dwarf will be conserved as it collapses to form a neutron star. Ignoring the geometry of the magnetic field, the product of the magnetic field strength and the area of the star's surface remains constant:

$$B_i 4\pi R_i^2 = B_f 4\pi R_f^2 \tag{16.28}$$

While this would require knowledge of the iron core's magnetic field and radius, comparisons with white dwarfs are common. Neutron star magnetic fields are typically on the order of 10^8T.

Neutron Star Temperatures

Neutron stars are extremely hot when first formed due to the whole supernova thing, with $T \sim 10^{11}$K. During the first day, the neutron star cools by emitting neutrinos via the **URCA process**, in which antineutrinos are created by a neutron decaying into a proton and electron, and neutrinos are created by the proton and electron combining. The neutrinos and antineutrinos fly unhindered into space, taking energy with them and consequently cooling the star. This occurs only when the nucleons aren't degenerate, which no longer applies after a day in which the star has cooled to $T \sim 10^9$K. Other neutrino process continue to dominate for the first thousand years until the neutron star is $T \sim 10^8$K, with a surface temperature of several million K. After such a time, the neutron star hovers around 10^6K and cools at essentially constant radius.

16.7 - Pulsars

General Characteristics

Pulsars are designated PSR, and all known pulsars share the following characteristics:

- Most pulsars have periods between 0.25 and 2s, with the average time being 0.795s.
- Pulsars have extremely well defined pulse periods (comparable in accuracy to atomic clocks).
- The periods of pulsars increase very gradually as the pulses slow down, the rate of increase being given the period derivative $\dot{P}$. Typically, $\dot{P} \sim 10^{-15}$.

Possible Pulsar Models

There are three obvious ways of obtaining rapid regular pulses in astronomy:

1. **Binary stars**. If the orbital periods of a binary star system are to fall in the range of the observed pulsar periods, then extremely compact stars must be involved (white dwarfs or neutron stars). This is ruled out, since the required separation falls below the radii of white dwarfs, and general relativity postulates that gravitational waves carry energy *away* from the binary which would imply the periodicity decreases − contradicting observations.
2. **Pulsating stars**. White dwarfs oscillate (non-radial g-modes) with periods between 100 and 1000s. It could be imagined that radial oscillation is involved with the pulsars, but the period for the radial fundamental node is a few seconds − much too long. A similar argument can eliminate neutron star oscillations, as the density implies neutron stars would oscillate with a radial fundamental mode period of around 10^{-4}s − much too fast for slower observed pulsars.
3. **Rotating stars**. The enormous angular momentum of a rapidly rotating compact star would guarantee clock-like behaviour. Suitably, the minimum rotation time comes out to be $P_{\min} \approx 5 \times 10^{-4}$s. Since this is the *minimum*, rotating stars could account for the observation of pulsars.

Evidence for a Core-Collapse Supernova Origin

Although at least one half of all stars are known to be members of multiple-star systems, only a few percent of pulsars are known to belong to binary systems. Pulsars also move much faster through space than do normal stars (sometimes in excess of 1000km/s). Both of these observations are consistent with supernova origins, since it's highly likely supernovae explosions aren't spherically symmetric and the forming pulsar could receive a 'kick' − possibly ejecting it from a binary system that it may have been apart of.

Synchrotron and Curvature Radiation

When relativistic electrons spiral along magnetic field lines, **synchrotron radiation** is produced as a continuous spectrum of light (or white light). From the equation of magnetic force on a moving charge q, $\mathbf{F}_m = q(\mathbf{v} \times \mathbf{B})$, and so the component of an electron's velocity $\mathbf{v}$ perpendicular to the field lines produces a circular motion around the lines, while the component of the velocity along the lines is not affected. As they follow curved field lines, the relativistic electrons accelerate and emit electromagnetic radiation in the direction of motion.
It is called synchrotron radiation if the circular motion around the field lines dominates, or **curvature radiation** if the motion is primarily along the field lines. In both cases, the shape of the continuous spectrum produced depends on the energy distribution of the emitting electrons and so is easily distinguished from the spectrum of blackbody radiation.
The radiation is strongly linearly polarized in the plane of the circular motion for synchrotron radiation and is strongly linearly polarized in the place of the curving magnetic field line for curvature radiation.

The Energy Source for the Crab's Synchrotron Radiation

The production of synchrotron radiation today requires both a replenishment of the magnetic field and a continuous injection of new energetic electrons. The total power needed for the accelerating expansion of the crab nebula, the relativistic electrons, and the magnetic field is calculated to be about 5×10^{31}W.
The energy source is the rotating neutron star at the heart of the Crab nebula. It acts as a huge flywheel and stores an immense amount of rotational kinetic energy. As the star slows down, its energy supply decreases.

The Structure of the Pulses

Pulses are brief and are received over a small fraction of the pulse period (typically from 1% to 5%). Generally, they are received at radio wave frequencies between roughly 20MHz and 10GHz.
A sharp pulse emitted at the neutron star, with all frequencies peaking at the same time, is gradually drawn out or *dispersed* by the interstellar medium as it travels to Earth. Because more distant pulsars exhibit a greater pulse dispersion, these time delays can be used to measure the distances to pulsars.
Although a typical pulse consists of a number of brief *subpulses*, the *integrated pulse profile*, an average built up by adding together a train of 100 or more pulses, is remarkably stable. Some pulsars have more than one average pulse profile and abruptly switch back and forth between them. The subpulses may appear at random times in the "window" of the main pulse, or they may mark across in a phenomenon known as *drifting subpulses*. Also, individual pulses may simply disappear or *null*, only to reappear up to 100 pulses later. Finally, the radio waves of many pulsars are strongly linearly polarized (up too 100%), a feature that indicates the presence of a strong magnetic field.

Magnetars and Soft Gamma Repeaters

Magnetars have magnetic field strengths on the order of 10^{11}T, several orders of magnitude larger than typical pulsars. They also have relatively low rotation periods of 5 to 8 seconds.
Magnetars were first proposed to explain the **soft gamma repeaters** (SGRs), objects that emit bursts of hard X-rays and soft gamma-rays. Each of the SGRs in the Milky Way (very few) are also known to correlate with young supernova remnants ($\sim 10^4$ yr), which would suggest that magnetars are short lived phenomena.
Magnetars are distinguished from ordinary pulsars by the fact that the energy of the magnetar's field plays the major role in the energetics of the system rather than the rotation.

13 Week 13 - Black Holes and Gravitational Wave Sources

17.1 - The General Theory of Relativity

The Curvature of Spacetime

Distances between points in space surrounding a massive object are altered in a way that can be interpreted as space becoming *curved* through a fourth spatial dimension perpendicular to *all* of the usual three spatial dimensions. Curved spacetime acts on mass, telling it how to move. Also, time runs more slowly in curved spacetime.

The Principle of Equivalence

To remove the noninertial effects of gravity and apply special relativity (which relies on inertial reference frames) to a gravitational potential, Einstein realized that local, infinitely small reference frames could remove the effect of gravity. In 1907, Einstein adopted this as a cornerstone of his theory of gravity:

The Principle of Equivalence: All local, freely falling, nonrotating laboratories are fully equivalent for the performance of all physical experiments.

Such "laboratories" are referred to as **local inertial reference frames**.

Gravitational Redshift and Time Dilation

Due to the curvature of spacetime in a gravitational potential, there exists an inherent redshift in light emitted from deeper within the potential well as measured from an observer further out. This **gravitational redshift**, that decreases the frequency of light as it travels upward a distance h out of the well (of instantaneous acceleration of g), is given by

$$\frac{\Delta\nu}{\nu_0} = -\frac{v}{c} = -\frac{gh}{c^2} \tag{17.6}$$

As the photon approaches infinity (out of the well) after starting at a radius (from the centre of the well) of r_0 and frequency ν_0, the exact result for the gravitational redshift (valid even for a strong gravitational field) is equal to that of the **gravitational time dilation**

$$\boxed{\frac{\Delta t_0}{\Delta t_\infty} = \frac{\nu_\infty}{\nu_0} = \left(1 - \frac{2GM}{r_0 c^2}\right)^{1/2}} \tag{17.13}$$

That is, a clock at r_0 runs more slowly than a clock at $r \to \infty$ since *time passes more slowly as the surrounding spacetime becomes more curved*. Gravitational redshift is a consequence of time running at a slower rate near a massive object.

7.2 - Intervals and Geodesics

Worldlines and Light Cones

In spacetime diagrams, time is represented on the vertical axis, while space is depicted by the horizontal $x - y$ plane. Since the third axis, z cannot be shown in 3D, depictions in this text only deal with motion in a plane.
The path follows by an object as it moves through spacetime is called its **worldline**. Photons travelling in the $x - y$ plane form a **light cone** that represents a widening series of horizontal circular slices through the expanding spherical wavefront of light. Spacetime diagrams are typically scaled so that the worldlines of photons make 45° angles with the time axis.
A massive object initially at event A must travel slower than light, and so it will subtend an angle between its worldline and the time axis less than 45°. Thus, the region inside the light cone represents the possible future of event A. Extending the diverging photon worldlines to the negative time axis shows the possible past influences on the event A (all of the events that could arrive at the location of event A as it happens). Outside of these lightcones are spacelike separated events − the region of spacetime that can have no influence on and not be influenced by the event A.
In principle, every event in spacetime has a pair of lightcones extending from it.

Spacetime Intervals, Proper Time, and Proper Distance

The analogous measure of "distance" in spacetime is called the **spacetime interval**, which is invariant under a change of reference frames (including Lorentz transformations), defined (for two events A and B) by

$$(\Delta s)^2 = c^2(t_B - t_A)^2 - (x_B - x_A)^2 - (y_B - y_A)^2 - (z_B - z_A)^2 \tag{17.16}$$

The value of $(\Delta s)^2$ corresponds to three distinct phenomena:

- If $(\Delta s)^2 > 0$, the interval is *timelike* and light can travel between events with time to spare.
- If $(\Delta s)^2 = 0$, the interval is *lightlike* or *null* and so light has exactly enough time to travel between the two events.
- If $(\Delta s)^2 < 0$, the interval is *spacelike* and light cannot travel between the two events.

By definition, the time between two events that occur at the same location is the **proper time**, where

$$\Delta\tau \equiv \frac{\Delta s}{c} \tag{17.17}$$

Also by definition, the distance measured between two events in a reference frame for which they occur simultaneously ($t_A = t_B$) is the **proper distance** separating them:

$$\mathcal{L} = \sqrt{-(\Delta s)^2} \tag{17.18}$$

This is essentially the rest length of some object or distance.

The Metric of Flat Spacetime

A worldline between two events in spacetime is not required to be straight, and the two events can be connected by infinitely many curved worldlines. To measure the interval along a curved worldline (for two events with no mass present), the **metric for flat spacetime** is used:

$$(ds)^2 = (c\,dt)^2 - (d\ell)^2 = (c\,dt)^2 - (dx)^2 - (dy)^2 - (dz)^2 \tag{17.19}$$

which, in spherical coordinates is

$$(ds)^2 = (c\,dt)^2 - (dr)^2 - (r\,d\theta)^2 - (r\sin\theta\,d\phi)^2 \tag{7.21}$$

The interval measured along any timelike worldline divided by the speed of light is always the proper time measured by a watch moving along that worldline. The proper time is zero along a null worldline and is undefined for a spacelike worldline.
The interval on flat spacetime between two events is a *maximum* if the worldline is a straight line (i.e. the smallest possible velocity defines that worldline as the change in distance traversed is a minimum).

Curved Spacetime and the Schwarzchild Metric

The straightest possible worldlines are called **geodesics**, and are straight lines in flat spacetime but *always* curved in a curved spacetime. The paths followed by freely falling objects through spacetime are geodesics.
General relativity has three fundamental features:

- Mass acts on spacetime, telling it how to curve.
- Spacetime in turn acts on mass, telling it how to move.
- Any freely falling particle follows a geodesic through spacetime. For a massive particle, the geodesic has a maximum or a minimum interval, while for light, the geodesic has a null interval.

As an object moves through curved spacetime, its **coordinate speed** is the rate at which its spatial coordinates change. The metric that describes curved spacetime surrounding a spherical mass, M, is called the **Schwarzchild metric**:

$$\boxed{(ds)^2 = \left(c\,dt\sqrt{1-\frac{2GM}{rc^2}}\right)^2 - \left(\frac{dr}{\sqrt{1-\frac{2GM}{rc^2}}}\right)^2 - (r\,d\theta)^2 - (r\sin\theta\,d\phi)^2} \tag{17.22}$$

where

$$d\mathcal{L} = \sqrt{-(\Delta s)^2} = \frac{dr}{\sqrt{1-\frac{2GM}{rc^2}}} \tag{17.23}$$

This shows that the spatial distance $d\mathcal{L}$ between two points on the same radial line is *greater* than the coordinate difference dr (think stretched grid lines around the massive object). The Schwarzchild metric also incorporates time dilation and the gravitational redshift, where $d\tau$ is equal to the first time in the equality in Eq (17.22). Since $d\tau < dt$, this shows that time passes more slowly closer to the massive object.

17.3 - Black Holes

The Schwarzschild Radius

For the simplest case of a nonrotating star, the radius of the black hole that would be created after gravitational collapse is the Schwarzchild Radius:

$$\boxed{R_S = \frac{2GM}{c^2}} \tag{17.27}$$

Spacetime behaves strangely at and beyond this radius, with the proper time measured by a clock at the Schwarzschild radius measuring $d\tau = 0$; time comes to a complete stop from the perspective of an observer far away from the event horizon. i.e. from an outside observer, *nothing ever happens at the Schwarzchild radius.*

The apparent speed of light, the rate at which the spatial coordinates of a photon change, is called the *coordinate speed of light.* At $r = R_S$, $dr/dt = 0$ for light and so light is frozen in time precisely at the Schwarzschild radius. This radius acts as a barrier that prevents any information from within the event horizon from escaping. Note that the event horizon is a mathematical boundary and does not coincide with any physical surface.

A nonrotating black hole has a particularly simple structure, with a **singularity** (a point of infinite density) at the center. Spacetime is infinitely curved at this singularity, and can never be observed due to the aforementioned event horizon.

A Trip into a Black Hole

Perspective of an Observer: According to a distant observer, an object will *never* reach the event horizon. In more detail, consider a flashing light source falling into a black hole. As it gets closer to the event horizon, a distant observer will record longer periods between flashes both due to the objects' increased speed (special relativity) and it being deeper in the gravitational well (general relativity). Furthermore, the coordinate speed of light becomes slower as the object approaches the black hole and so the signals travel to the observer more slowly. Due to both the acceleration 'away' and gravitational redshift, the signal flash is intensely redshifted also. The flashing appears to become less intense also due to the rate at which the photons escape the object declines (according to the observer) and the energy of each photon decreases. Eventually, the light is redshifted and dimmed into invisibility as time dilation brings the objects coordinate speed to zero.

Perspective of the Object: Because gravity has been abolished in the object's reference frame, the approach to the black hole brings no noticeable effects (the proper time progresses smoothly and the flashing is consistent). As the object gets very close to the black hole, *tidal forces* become significant (more force closer to the event horizon than further away). As this happens, the local inertial frame of the object becomes smaller as the spatial variation in the gravitational acceleration vector, $\mathbf{g}$, increases.
Once past the event horizon, $r < R_S$, it is impossible for the object to be at rest. Inside the event horizon, the elapsed coordinate time in the outside world becomes infinite, and the light from much of (but not all of) the "future" reaches the object from above as it falls towards the singularity.

Mass Ranges of Black Holes

Stellar-mass black holes with masses in the range of 3 to $15M_\odot$ or so, may form directly or indirectly as a consequence of the core-collapse of a massive star. The direct collapse of the core to a black hole may be responsible for the production of collapsar (gravitational-collapse remnant), whereas a delayed collapse of a rapidly rotating neutron star may result in a supranova (Gamma Ray Burst followed by collapse to a black hole). It is also possible that a neutron star in a close binary system may gravitationally strip enough mass from its companion that the neutron star's gravity exceeds the degeneracy pressure to support it, resulting in a black hole.

Intermediate-mass black holes (IMBHs) may exist that range from roughly 100 to $1000M_\odot$. Evidence for them exists in the detection of ultraluminous X-ray sources. The correlation of IMBHs with the cores of globular clusters and low-mass galaxies suggest that they may develop from the mergers of stars (to form collapsing supermassive stars), or by the merger of stellar-mass black holes.

Supermassive black holes (SMBH) are known to exist at the centers of most galaxies. They range from 10^5 to $> 10^9 M_\odot$ and could have formed from galaxy mergers, or perhaps as an extension of the formation process of IMBHs.

Primordial black holes are thought to have been created shortly after the big bang, and with a range of masses from 10^{-8}kg to $10^5 M_\odot$.

Black Holes Have No Hair!

Since the core-collapse of a star is almost certainly not symmetrical, one might expect a black hole to not satisfy radial symmetry, but any irregularities are radiated away by gravitational waves and once the surface of a star reaches the event horizon, the exterior spacetime horizon is spherically symmetric.
Any black hole can be completely described by just three numbers: it's mass, angular momentum, and electric charge. This simplicity is often referred to as "black holes having no hair".
There is a firm upper limit on the angular momentum of a rotating black hole:

$$L_{\max} = \frac{GM^2}{c} \tag{17.29}$$

If a black hole were to exceed this limit, there would be no event horizon and a naked singularity would appear (which violates the Law of Cosmic Censorship).

Spacetime Frame Dragging

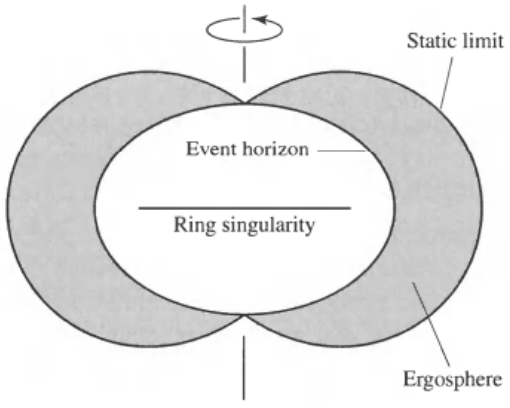

Figure 17.22: Structure of a Maximally Rotating Black Hole

In a maximally rotating black hole, the rotation distorts the singularity from a point into a flat ring, and the event horizon assumes the shape of an ellipsoid. As a massive object spins, it induces a rotation in the surrounding spacetime in a phenomenon known as **frame dragging**. Near a rotating black hole, frame dragging is so severe that there is a nonspherical region outside the event horizon called the **ergosphere** where any particle *must* move in the same direction that the black hole rotates. Spacetime within the ergosphere is rotating so rapidly that a particle would have to travel faster than light to remain at the same angular coordinate. The outer boundary of the ergosphere is called the **static limit** (named because beyond this boundary, a particle can remain at the same coordinate as the effect of frame dragging diminishes.

Hawking Radiation

Black holes can slowly *evaporate* through a process of pair production, where a particle–antiparticle pair form just outside the event horizon. Ordinarily the particles would quickly recombine, but if one of the particles falls into the event horizon while the partner escapes, the black hole loses the energy used to create one of the particles. The net effect as seen from a far away observer is the emission of particles by the black hole, known as **Hawking radiation**, accompanied by a reduction in the black hole's mass.

The rate at which energy is carried away by particles in this manner is inversely proportional to the square of the black hole's mass. For stellar-mass and above black holes, the emitted particles are photons and the rate of emission is minuscule. As the mass declines, however, the rate of emission increases and the final stage of a black hole's evaporation proceeds extremely rapidly, releasing a burst of all types of elementary particles. This explosion leaves behind only an empty region of flat spacetime.
The lifetime of a primordial black hole prior to its evaporation, t_{evap}, is quite long:

$$t_{\text{evap}} = 2560\pi^2 \left(\frac{2GM}{c^2}\right)^2 \left(\frac{M}{h}\right) \approx 2 \times 10^{67} \left(\frac{M}{M_\odot}\right)^3 \text{ yr} \tag{17.30}$$

By this equation, primordial black holes with a mass of about 1.7×10^{11}kg should be in the final, explosive stage of evaporation right now. The final burst of Hawking radiation is thought to release high energy gamma rays at a rate of 10^{13}W together with many other particles. To date, measurements of the cosmic gamma-ray background at this energy have not detected anything that can be identified with the demise of a nearby primordial black hole. This negative result implies that there cannot be more than 200 primordial black holes of this mass in every cubic light-year of space (due to the sensitivity of equipment used to detect them).

Gravitational Waves

Anatomy of Gravitational Wave Detections

The interaction of two dense, closely orbiting objects causes ripples in spacetime that radiate outwards into the universe. The first concrete detection of gravitational waves involved observation of a "chirp" caused by the inspiralling binary of two black holes that merged (of about 29 and 36 solar masses) and released three solar masses worth of *energy* in a few tenths of a second. This energy release event was, for a short moment, many times more energetic than the collected light of all the stars in the visible universe.

The first inference of gravitational waves occurred in the 1970s when binary pulsars were observed to fall towards each other at an increasing speed. To do this, they had to lose gravitational energy in the form of gravitational waves, and the observations aligned perfectly with that predicted by general relativity. As dense binary objects coalesce towards each other, the frequency and amplitude of their emitted gravitational waves increase, referred to as a "chirp" in their output.

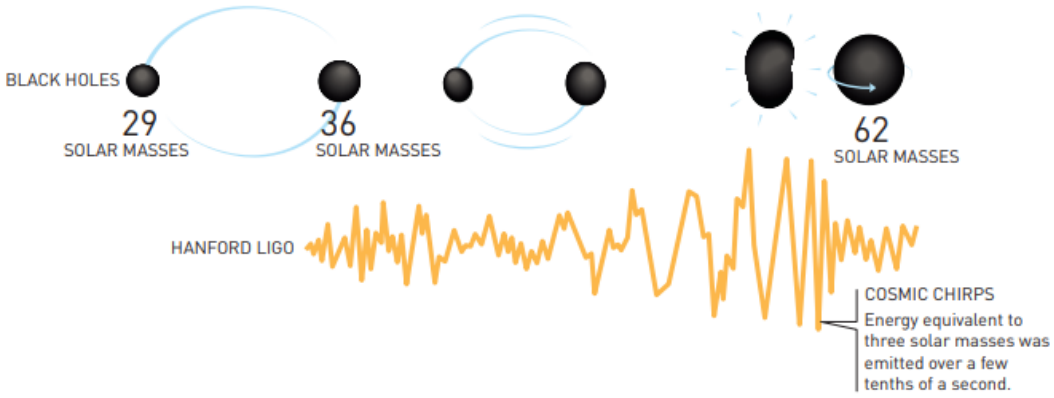

Figure 27: First LIGO Detection of Gravitational Wave Chirp, with Associated Black Holes

Sources of Gravitational Waves

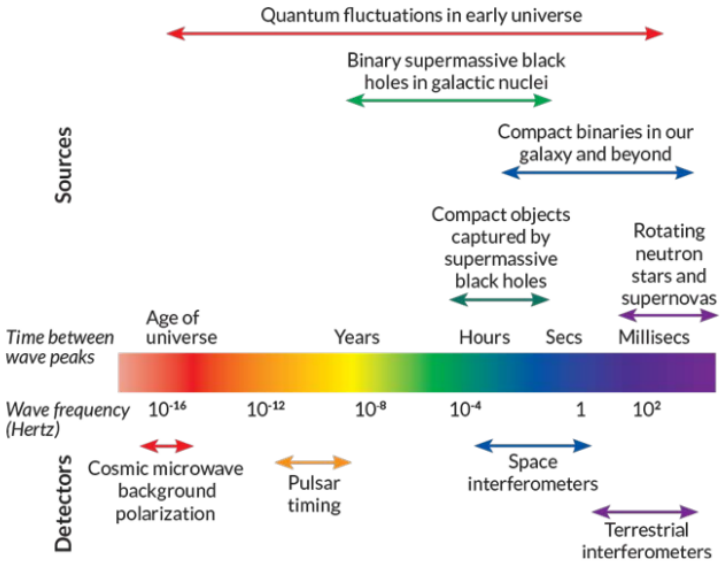

Figure 28: Gravitational Wave Spectrum

In general terms, gravitational waves are emitted by accelerated objects whose motion is not spherically symmetric.
Short lived and fairly well-modelled sources of gravitational waves generally include compact objects in tight orbits (such as with neutron stars, etc). The sequence of inspiral and merger gives rise to a characteristic signal (the "chirp"), which dies down as the final object 'rings down'.
Short-lived and poorly known sources such as supernovae are expected to produce some gravitational waves provided there is some asymmetry in the core collapse.
Long lived, diffuse sources of gravitational waves include the primordial background of gravitational waves predicted by most cosmological theories.

The First Detection and LIGO

The apparatus used to measure gravitational waves to a sufficient sensitivity is a laser-based interferometer, with two long arms that form an L shape. At the corner and the ends of the L, massive mirrors are suspended in a sophisticated device, where traversing gravitational waves stretch one arm and compress the other. This tiny change in length between the arms results in the lasers being projected through the arms becoming out of phase which creates a signal in a photodetector at the intersection of the arms (where there would otherwise normally be no signal due to the superposition of the lasers totally destructively interfering). The arm lengths of 4km allow for detections of compression or elongation to a degree smaller than an atomic nucleus.
Two LIGO sites and one Virgo interferometer are currently in operation (two 3000km apart in the US, and another in Italy), and using the delay in signal detection between them allows for a *rough* estimation as to the location of the source event; the location of which is then investigated using optical telescopes and/or observatories.

Merging Neutron Stars and Kilonovae

Shortly after the Virgo (Italian) laser interferometer came online, a weak detection of a gravitational wave chirp sent astronomers looking at the galaxy NGC 4993, about 140 million light years away where the merger of two neutron stars was predicted to occur. What they observed, right where the gravitational waves appeared to originate from, was a **kilonova**: the merger of two neutron stars which produces intense gamma-rays and strong EM radiation across the whole spectrum as a result of r–process nucleosynthesis, on the order of 1000 times a nova luminosity (or 1/10 to 1/100 that of a core-collapse supernova). These kilonova are thought to be responsible for a significant proportion of the very heavy elements in the interstellar medium.

As the neutron stars spiral closer to each other, tidal forces are thought to break one or both of them apart into a sort of accretion disk (or unstable taurus) which induces relativistic jets perpendicular to the plane of rotation that leads to *short* gamma-ray bursts.
If both of the stars are tightly gravitationally bound, they may immediately coalesce into a black hole which would prohibit any exterior material to produce a kilonova or gamma-ray burst.
If both neutron stars are weakly gravitationally bound, they may combine into a rapidly spinning super-massive neutron star which could produce a gamma-ray burst after a holdup of tens or hundreds of seconds.
The most likely case is somewhere between with the aforementioned accretion disk or unstable taurus shaped neutron star that eventually collapses to form a black hole (not before causing a kilonova).

Since these events are hypothesized to be extremely consistent in comparison with one another, both in terms

of duration and luminosity, they may act as a "standard-signal" in cosmology to help calculate redshift over cosmological distances. Initial calculations using the NGC 4993 neutron star merger provide results that agree excellently with established results for universe expansion and the age of the universe.